Master's thesis

NTNU
Norwegian University of Science and Technology
Faculty of Natural Sciences
Department of Materials Science and Engineering

Kristine Fagerheim

Structure and phase transitions of A_2MBr_4 supramolecular crystals where A=[$N(CH_3)_4$] and/or [$N(C_2H_5)_4$] and M= Zn or Mn

Master's thesis in Chemical Engineering and Biotechnology

February 2021

NTNU
Norwegian University of Science and Technology

Kristine Fagerheim

Structure and phase transitions of A_2MBr_4 supramolecular crystals where A=[$N(CH_3)_4$] and/or [$N(C_2H_5)_4$] and M= Zn or Mn

Master's thesis in Chemical Engineering and Biotechnology
February 2021

Norwegian University of Science and Technology
Faculty of Natural Sciences
Department of Materials Science and Engineering

NTNU
Norwegian University of
Science and Technology

Structure and phase transitions of A_2MBr_4 supramolecular crystals where A=$[N(CH_3)_4]$ and/or $[N(C_2H_5)_4]$ and M= Zn or Mn

TMT4900: Material chemistry and energy technology,
Master thesis

Kristine Fagerheim
Candidate number: 10002

Supervisors:
Prof. Mari-Ann Einarsrud
Dr. Julian Walker

Department of Material Science
Norwegian Univeristy of Science and Technology
Spring 2021

-

Preface

This thesis is part of the course TMT4900 Material chemistry and energy technology, Master thesis. The work is a continuation of the work carried out in the course TMT4500 Material chemistry and energy technology, Specialisation project, which is described in the report: Organic-inorganic supramolecular plastic crystals[1].

I want to thank my supervisor Prof. Mari-Ann Einarsrud and co-supervisor Dr. Julian Walker for excellent supervising and encouraging mails throughout this whole process. I also want to thank my fellow students for making the time as a student my best. At last, but not least, I want to thank my family for all support and for always believing in me.

Abstract

The need for smaller, more sustainable and flexible electrical devices have increased the interest to find replacements for the conventional metal oxide ferroelectrics which are generally brittle and have a non-energy effective production. However, plastic crystals, a type of supramolecular materials, exhibit a mesophase which makes shaping and processing at moderate temperatures possible. In this regard six new compositions, A_2MBr_4 where A = $[N(CH_3)_4]$ and/or $[N(C_2H_5)_4]$ and M = Zn or Mn, of organic-inorganic crystals were made through a crystallization method starting with an aqueous solution followed by slow evaporation at room temperature. The aim for this project was to understand how the composition influenced the structure so that we might better understand how to tune structure-properties of these materials. For this purpose, the final products were characterized by X-ray diffraction(XRD) and differential scanning calorimetry (DSC). The XRD analysis was done to determine the structure of the compositions while the DSC analysis determined the phase transitions during cooling and heating of the materials and the enthalpy was calculated to determine the energy used in the transition. The results showed that:

- The cation size had a large effect on the structure of the materials, effectively changing the symmetry and space group of the material.
- The anion used had a noticeable but smaller effect, producing a volume change in the unit cell corresponding to the anion size.
- A complex array of phase transitions was observed between -25 and 280 °C displaying both order-disorder and displacive characteristics depending on the composition. The organic cation played the largest role in influencing this behaviour.

Sammendrag

Behovet for mindre, mer bærekraftige og elastiske elektriske innretninger har økt interessen for å finne erstatninger for konvensjonelle ferroelektriske materialene som ofte er sprø og har en lite energieffektiv produksjon. Imidlertid har plastiske krystaller vist, en type supramolekylære materialer, en mesofase som muliggjør forming og bearbeiding ved moderate temperaturer. I den forbindelse har seks nye komposisjoner, A_2MBr_4 hvor A = $[N(CH_3)_4]$ og /eller $[N(C_2H_5)_4]$ og M = Zn eller Mn, av organisk-uorganiske krystaller blitt fremstilt gjennom en krystalliseringsmetoden som starter med en vandig løsning etterfulgt av langsom fordampning ved rom temperatur. Målet for dette prosjektet var å forstå hvordan komposisjonen påvirket strukturen og dermed hvordan strukturegenskapene til disse materialene kan justeres. For dette formålet ble sluttproduktene karakterisert ved røntgendiffraksjon (XRD) og differensial skanningskalorimetri (DSC). XRD analyse ble gjort for å bestemme strukturen til komposisjonene, mens DSC analysen bestemte faseovergangene under kjøling og oppvarming av materialene. Entalpi ble beregnet for å bestemme energien som ble brukt i overgangene. Resultatene viste at:

- Kationstørrelsen hadde en stor effekt på materialets struktur, og endret materialets symmetri og romgruppe.
- Anionet som ble brukt, hadde en merkbar, men mindre effekt, og ga volumendring i enhetscellen som tilsvarte anionstørrelsen.
- Et komplekst utvalg av faseoverganger ble observert mellom -25 og 240 °C som viste både endring i orden-uorden og forflyttinger i strukturen som følge av endring i komposisjonen. Det organiske kationet hadde den største påvikningen på disse endringene.

Contents

List of Abbreviations

A_2MBr_4	General formula for the compounds in the thesis
A	$[N(CH_3)_4]^+$ and/or $[N(C_2H_5)_4]^+$
M	Zn or Mn
XRD	X-ray diffraction
DSC	Differential scanning calometri
TMA	Tetramethylammonium: $[N(CH_3)_4]^+$
TEA	Tetraethylammonium: $[N(C_2H_5)_4]^+$
ΔG	Difference in Gibbs energy
H	Enthalpy
S	Entropy
ΔG_v	Difference in Gibbs energy between liquid and solid phase
ΔG^*	Critical change in Gibbs free energy
r^*	Critical radius
$\dot{G}$	Growth rate
Q	Activation energy
C	Diffusion coefficient
T_m	Melting temperature
d_{hkl}	Interplanar spacing
β	Monoclinic angle
T_c	Transition temperature
TMABr	Tetramethylammoniumbromide
TEABr	Tetraethylammoniumbromide
$ZnBr_2 \cdot 2\,H_2O$	Zinc bromide dihydrate
$MnBr_2 \cdot 4\,H_2O$	Manganese bromide tetrahydrate
GOF	Goodness of fit
H_{fus}	Enthapy of fusion
Ucv	Unit cell volume

1 Background

1.1 Motivation

Since the discovery of ferroelectricity in 1921, the ferroelectric materials have grown into a commercial industry and become a major field of research due to their useful range of properties. These materials exhibit a spontaneous electric polarisation that is switchable by application of an electrical field. Nowadays, they are used in a wide range of everyday applications such as mobile phones, sensors and capacitors. Ferroelectric ceramics, with their excellent piezoelectric coefficient, dielectric constant and stability thermally and atmospherically, have been the most used ferroelectric material since their discovery in 1940 with barium titanate ($BaTiO_3$) as the pioneer[2]. However, the demand for more sustainable and flexible materials for next generation electronics are not compatible with the brittleness and the high processing temperature of the ceramics. Therefore, another group of ferroelectrics, the hybrid organic-inorganic plastic crystals, have gained attention. These materials are lightweight, flexible and have a moderate processing temperature[3].

The main attraction about the plastic crystal ferroelectrics are the combination of a shapeable plastic crystal phase at moderate temperatures and a possible ferroelectric phase at room temperature. The plastic crystal phase is a mesophase which is a intermediate solid-liquid state where the molecules are fixed at a given position in the crystal lattice but, in addition, do have the freedom to rotate at this position[4]. These possible transnational motions allows the material to flow under stress hence the name plastic crystals. Materials exhibiting this plastic crystal mesophase are referred to as supramolecular materials which are made of globular molecules[5]. This indicates that the material consists of molecular ions which makes it suitable as a more sustainable alternative as it is easier to tailor the material properties without increasing the number of elements used in the composition.

In the light of sustainability the plastic crystals are favourable compared to the commercial metal oxides. The possibility to use fewer elements in the synthesis of the materials as well as more use of abundant elements such as carbon, nitrogen and hydrogen makes these materials interesting from an environmental perspective. The synthesis of the plastic crystal ferroelectrics is potentially less technically challenging due to the low temperatures involved, which also allow for potential cost and energy savings, relative to conventional metal oxides which require high temperatures (e.g. 1000°C) for synthesis.

The field of research regarding plastic crystal ferroelectrics is still developing. The relationship between the chemical structure of the cations or anions and the physical properties of the final structure are still not clear[3]. This is important information to be able to optimise the synthesis and to develop new ferroelectric plastic crystals with desired properties.

Figure 1.1: Super-flexible plastic crystal device for bendable displays[?] .

Previous research on A_2MBr_4 supramolecular crystals where A=$[N(CH_3)_4]^+$ and/or $[N(C_2H_5)_4]^+$ and M= Zn or Mn have reported several phase transitions at moderate temperatures which makes these materials interesting in the field of plastic crystals. However the influence of the cations and anions on the crystal growth, crystal structure and the characteristic of the phase transitions has not yet been well studied and the current study wishes to address this knowledge need.

1.2 Aim of work

The aim of the work is to understand how different cations and anions influence the A_2MBr_4 structure. The goal is to achieve this by exploring the synthesis and structure of different organic-inorganic supramolecular materials with the possibility of a plastic mesophase at moderate temperature and a possible ferroelectric/ferroelastic phase around room temperature. To achieve this goal crystal growth was observed from aqueous solutions, the structures was studied via X-ray diffraction (XRD) and Differential scanning calorimetri (DSC) was used to identify phase transitions as a function of temperature.

By combining two different cations, $[N(CH_3)_4]^+$ and $[N(C_2H_5)_4]^+$, with different two anions, $[ZnBr_4]^{2-}$and $[MnBr_4]^{2-}$ to six compositions it is possible to study how the cations and anions influence the crystal growth, crystal structure and the identity of the phase transitions.

2 Introduction

This thesis treats the synthesis and characterization of six compounds with the composition A_2MBr_4 where A=$[N(CH_3)_4]^+$ (hereafter TMA) and/or $[N(C_2H_5)_4]^+$ (hereafter TEA) and M= Zn or Mn. To make the reader familiar with the topic, the introduction will touch upon relevant topics organised in the following subheadings: Supramolecular materials, Crystallization and A_2MBr_4 crystals.

2.1 Supramolecular materials

Supramolecular chemistry offers a strategy for designing new materials[6]. The formation of supramolecular materials is driven by a non-covalent nature of the interactions which makes it possible to tune the material properties[5]. These systems are prepared by processes as molecular recognition, self-assembly and self-organization, in crystalline and solid state by mulitcomponents[7]. However, it is the process of self-assembly that makes it possible to design a supramolecular crystal with desired properties.

As they are crystals, the structure is highly ordered with a periodically extended supramolecular lattice in three directions. The motif (building block), which repeats itself in the lattice, holds many molecules which usually do not have specific atomic/molecular positions to generate a repetition scheme in the motif. In other words, at the length scale of motif repetition, long-range orders are retained with respect to positional, bond-orientational and molecular-orientational matters. However, molecules and/or clusters within the motifs do not retain either long-range, quasi-long range or short range order. Thus, the supramolecular crystals ordered structures are constructed on the basis of the motifs repeatability. This is in contrast to for example protein crystals which perfectly retains each atomic position[8].

The crystallization mechanism for the supramolecular crystals is similar to the one for smaller compounds. They undergo a phase transition which involves nucleation and growth. However, in the structure formation of these type of crystals there will be stages of sequential ordering as there will be hierarchical structures at different length scales[8]. When the size and mass of the motifs increase the dynamics becomes more sluggish. Therefore, in some cases, external force fields are used to overcome the free energy barrier to continue the crystal growth. Often, the supramolecular crystallization ends in a metastabe state which is not thermodynamidally the most stable state[8].

2.1.1 Plastic crystals

Plastic crystals are supramolecular materials with molecular ions occupying positions of the crystal lattice instead of single element ions. The term plastic crystal was first used by Timmermans in 1935 when he discovered an extensive series of cubic mesophases[4]. These crystals have the desirable combination of properties of dielectric, piezoelectric and ferroelectric at room temperature[9]. These crystals are generally formed by globular, symmetrical around their centre or gives a sphere around an axis by rotation[4], shaped molecules. The geometry of the molecules leads to a small steric hindrance for reoriental process which again leads to a high plasticity.

As mentioned, the plastic crystals shows a mesophase which is a combination between the liquid and the ordered crystal phase (Figure 2.1). In the liquid phase, the molecules are free to move while in the ordered crystal phase they are strongly bonded without freedom to move. As for the plastic crystals, the molecules are ordered like a crystal but they exhibit rotational freedom. While being in the mesophase, the crystals plastically deforms easily due to the possibility of transnational motions in the lattice[3].

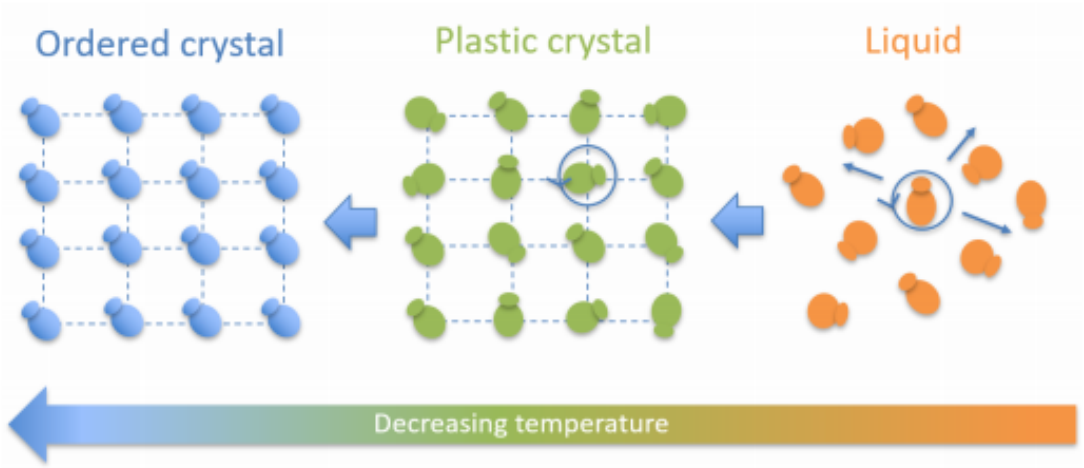

Figure 2.1: Plastic crystal phases are mesophases which possess properties in between the liquid and solid phases. They exhibit molecular rotational freedom and molecules fixed at certain positions in the crystal lattice[10].

Organic-inorganic plastic crystals have been attracting increasing interest due to their novel physical properties and a drive towards development of more sustainable ferroelectrics. The conventional ferroelectric materials, such as ceramics, have a high conductivity but are brittle and the manufacturing is energy-intensive. As the world of electronics develop and the desire for more flexible, smaller and more sustainable devices increase the need for new materials to arise. By using the principles in supramolecular chemistry, non-covalent interactions which are formed into ordered assemblies, it is possible to design new ferroelectric materials which are dynamic under the influence of an electric field. The two building blocks to design new organic ferroelectrics are bistable electronic dipoles and structural building blocks in the form of supramolecular assemblies with a non-centrosymmetric lattice[6]. The combination of these two generates the possibility of ferroelectricity. In this case, the interactions between the molecules are important to be able to switch the polarization. Supramolecular ferroelectrics are designed by organization of induviduvidual molecules into ordered lattices which needs to be dynamic under influence of an electric field[6]. Ferroelectric materials are one of the most used and studied polar crystalline materials[11]. The interest in these materials originate from the exhibition of a spontaneous polarization which is reversible by application of an electric field. Their excellent piezoelectric coefficients and dielectric constants are important properties for use in electronics such as sensors, transducers, capacitors and actuators[9].

The magnitude of the polarization depends on the direction of the ferroelectric axis in the material. For polycrystalline ferroelectrics, which consists of aggregates of single-crysta grains, the polarization directions are random which can increase the magnitude of the polarization after poling and the switching of the polarization can be done more easily compared to a single-crystal ferroelectric. Due to this fact an important property of these materials are the number of equivalent polarization directions which is dependent on the change of symmetry between the high temperature paraelectric phase and the low temperature ferroelectric phase. In this matter, the plastic phases are interesting due to their high symmetry and the ability to transform to stable low symmetric phases[11]. Plastic phases exhibit a lot of interesting properties but these transitions are rarely induced in ferroelectrics. However, Ye et al.[11] have reported a molecular-ionic ferroelectric compound, tetraethylammonium perchlorate, with a plastic phase transition and 12 equivalent ferroelectric axes. The plastic phase usually crystallizes in a highly symmetric cubic system which gives rise to the appearance of this many equivalent ferroelectric axes[11].

A type of plastic crystals are the ionic plastic crystals which are ionic compounds where the anion and cation are molecular ions. These compounds have shown to possess properties which has given rise to increased interest in the development of high conductivity solid state electrolytes for use in devices like batteries, solar cells and fuel cells as Pringe *et al*[3]. emphasises in their study of these materials[3]. The desired property, in this case, of plasticity originates from the possibility to flow under stress which arise from the translational motions in the material. Thus, in electrochemical devises, the plasticity of the material make the contact between the electrolyte and the electrodes during possible changes in volume[3]. Pringe et al. underlines the difficulty to predict which combinations of cations and anions which will make plastic crystalline materials. In the study several salts were compared and the importance of the cation structure were indicated as being important to determine plasticity.

2.1.2 Phase transitions

Compounds with the general formula A_2MBr_4, where A is $[N(CH_3)_4]$ and/or $[N(C_2H_5)_4]$ and M= Zn or Mn, often exhibit phase transitions leading to a ferroelectric or ferroelastic crystal ordering[12]. A phase transition is a transition from a phase to another that often possess other properties. The most common phase transitions are liquid-gas, solid-liquid and solid-gas[13]. In addition, there are several other types of phase transitions as in this project where the materials undergo solid-solid phase transitions[14]. Paul Ehrenfest made a classification for phase transitions with respect to the change in the thermodynamic functions in the transition. In Ehrenfest classification, the phase transitions are denoted first- or second-order phase transitions which depends on how Gibbs energy changes with respect to the temperature in the phase transition. Gibbs energy, ΔG, is a thermodynamic parameter consisting of information about the internal energy of the system, enthalpy, H, and the measurement of disorder of the atoms, entropy, S. The definition on a first-order phase transition is continuous Gibbs energy throughout the phase transition while the derivative of Gibbs energy discontinuous. This leads to a jump in volume, entropy and enthalpy during the phase transition. However, a second-order phase transition is defined by a continuous first derivative and a discontinuous second derivative of Gibbs energy with respect on temperature. This leads to continuous volume, enthalpy

and entropy during the phase transition[14].

In the study of phase transitions in molecular crystals several examples of dynamic crystals are revealed which responds to temperature with mechanical motion such as translation, rotation and bending to name a few. During the heating of the material, the atoms will gain energy leading to the atoms having enough energy to break out from their rigid, at a given solid to liquid temperature, structure they are obtaining in the solid state. The process of breaking the structure down from a rigid to a less rigid one gains energy to the material and are therefore called an endothermic transition. The opposite transition, as for example crystallization, is an exothermic transition which is energy released from the material.

2.2 Crystallization

This section was fist published in Specialization project "Organic-inorganic supramolecular plastic crystals"[1]. Crystallization is the natural process of solidification from a liquid. It often occurs due to physical changes like temperature or density. Crystallization is an widely used laboratory technique and is often used to purify substances or, in combination with advanced imaging techniques, to get information about the properties of the substance crystallized. Crystallization may be divided into two steps; nucleation and growth.

2.2.1 Nucleation

Crystallization starts by the formation of small solid particles which increase in size as the phase transition goes on to completion. The phase transition can be divided into two stages: nucleation and growth[15]. Homogeneous nucleation is defined as the uniform formation of the new phase throughout the parent phase. An important parameter when it comes to phase transitions is the free energy, ΔG which is a thermodynamic parameter consisting of information about the internal energy of the system, enthalpy H, and the measurement of disorder of the atoms, entropy S. The nucleation can only happen spontaneously if ΔG has a negative value. Formation of nuclei of the solid phase occur in the interior of the liquid by clusting of atoms in arrangements similar to the one for the solid phase. Assuming nucleus with spherical geometry and a radius r. The total free energy has two contributions: the first one is the difference in free energy between the liquid and the solid phases, ΔG_v, and the volume of the nucleus while the second one is the origin from the formation of the boundaries between the liquid and solid phases. The total free energy change is in Figure 2.2 plotted against the radius of the nuclei while the two energy contributions are shown in red and blue where blue is the volume free energy and the red being the surface free energy. The green graph is a combination of the two contributions and shows the ΔG^* critical change in free energy, and the associated critical radius, r^*, which is the energy that have to be overcome for the nucleus to be able to grow as a form of activation energy. (embryo before r* and nucleus after). The green graph shows that in the first stage of atoms in the liquid cluster together a solid particle starts to form and the free energy is increasing while after the cluster reach the critical radius it will continue to grow accompanimented with an decrease in the free energy and form stable nuclei.

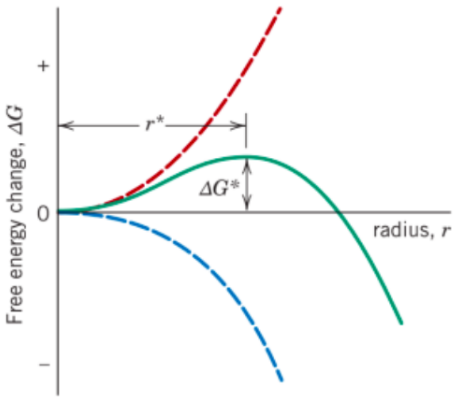

Figure 2.2: The total free energy change is plotted against the radius of the nuclei while the two energy contributions are shown in red and blue where blue is the volume free energy and the red being the surface free energy. The green graph is a combination of the two contributions and shows the ΔG^* critical change in free energy, and the associated critical radius, r^*, which is the energy that have to be overcome for the nucleus to be able to grow as a form of activation energy[15].

The number of stable nuclei is depending on the temperature and an increase in temperature will increase the activation free energy and decrease the number of stable nuclei.

2.2.2 Growth

The growth of the nuclei starts when the embryo has reached the critical size, r^*, and has become a stable nucleus. The growth of particles of the new phase will continue to occur simultaneously with nucleation in the regions where the phase transition not yet is completed. The growth rate, $\dot{G}$, is determined by the diffusion rate because the nucleation is generated by the diffusion of atoms in form of diffusion through the parent phase or across a phase boundary and into the nucleus. The dependence of particle growth rate on the activation energy for diffusion and temperature is given by the equation

$$\dot{G} = Cexp(-\frac{Q}{kT}) \tag{2.1}$$

where Q is the activation energy and C is the diffusion coefficient which are independent of the temperature. The size of the particles in the product phase depends on the tranformation temperature. At temperatures close to T_m the growth rate will be high while the nucleation will be low which indicates few nuclei form that grow rapidly. This will result in a microstructure consiting of few and large particles and at the opposite side at lower temperatures the microstructure will consist of many small particles[15].

The relation between the crystallization and dissolution are, under ideal conditions, equal at a given temperature and under equal concentration conditions. Therefore, the growth and dissolve rate of all faces in the crystals are equal. However, this is not the fact in practice where the crystals usually dissolve faster than they grow. The growth and dissolve

rates varies on the different faces which varies in different substances, concentrations, temperatures and purity[16].

2.2.3 Crystal habit

Predication of crystal morphology is an important field as materials with specific properties are required in industry which makes the knowledge of crystal habit desirable. The growth rate of different crystallographic faces decides the crystal morphology. The size of the faces can vary a lot within the crystal systems as shown in Figure 2.3 for a hexagonal crystal.

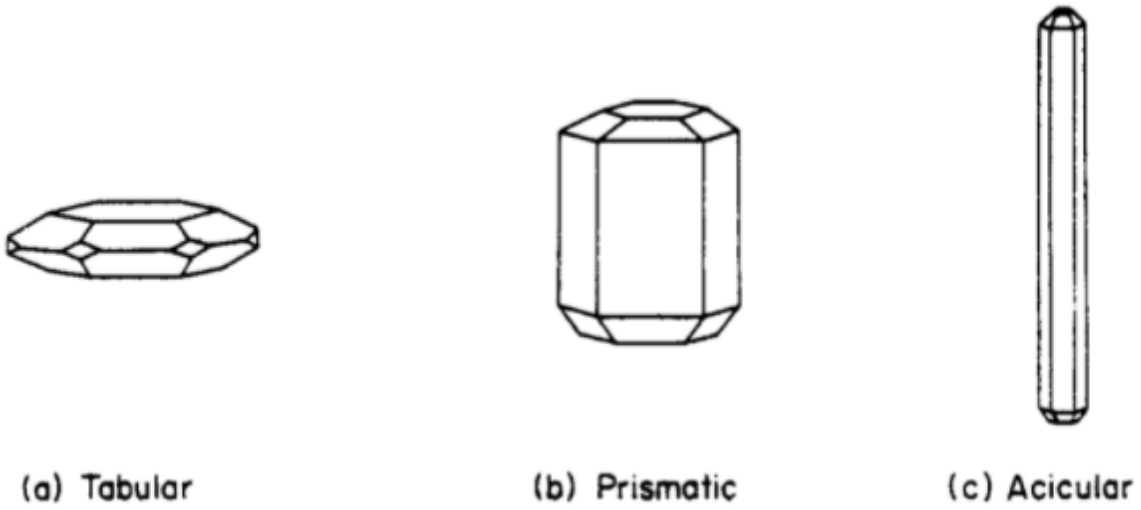

Figure 2.3: Three different modifications of crystal habits in a hexagonal crystal[16].

These differences in growth is called modification of habit. The growth can vary in the different directions and lead to elongated faces in one direction and stunted in another, as shown in Figure 2.3. However, this growth can often be controlled by several factors. Seeding of a supersaturated solution or sudden cooling can cause rapid crystallization and the formation of needle crystals. The state of agitation of the system is influenced by the degree of supersaturation and supercooling and will therefore affect the crystal habit. Impurities in the supersaturated solution can lower the growth rate in one direction and therefore also influence the growth rate. In crystal morphology the governing faces are the ones with the greatest interplanar faces, d_{hkl}, and highest reticular densities. This means the closest-packed faces and those with the lowest Miller indices have the slowest growth and are the most influential on the crystal morphology.In addition, the surface energy theory indicates that the equilibrium form of the crystal growth should be such that the surface energy per unit volume is at a minimum.

2.3 A_2MBr_4 crystals

In this section some previous research onA_2MBr_4 crystals, where A=TMA and/or TEA and M= Zn or Mn, are presented.

$TMA-MBr_4$
Crystals with the chemical formula TMA_2MBr_4 have gotten a lot of attention the past years due to their unusual phase transitions and possible ferroelastic and ferroelectric phases. The reorientational dynamics of the TMA groups contribute to the difference in successive structural phase transitions the crystals of this kind undergoes. The compounds with bromide as the halogen along with Zn or Mn show an unusual second-order phase transition around 0 °C from the high-temperature phase with an orthorhombic structure to the low-temperature phase with monoclinic structure of a ferrodistortive character[17].

The tetrabromide salts studied here have showed an anomalous behaviour of the monoclinic angle (β) below the transition temperature, T_c. When decreasing the temperature the monoclinic distortion increases below T_c, then goes up to a maximum value at T_m followed by a gradually decrease to zero at T_z (β=90°) and at lower tempratures becomes negative. This behaviour does not originate from a phase transition but can be explained by the presence of two independent sublattices competing with opposite signs and magnitudes on the straines. In general $TMA-MBr_4$ crystals exhibit three types of sublattices denoted TMA(1), TMA(2) and MBr_4 whereas the two cations is assumed to occupy two equivalent sites with equal probability[18].

$TMA-ZnBr_4$ undergoes a second order phase transition around 15 °C from the paraelastic phase with the space group *Pmcn* to a ferroelastic phase with the space group $P_{121/c1}$[19]. The lattice parameters at room temperature found by the refinement done by Asahi *et al* are given in Table 2.1. The unit cell consist of four units with two nonequivalent types of TMA cations and one type of $ZnBr_4$-ions which all are disordered symmetrically in the paraelastic phase[20].Iwata *et al*[21] have observed ferroelastic domains in single crystal $TMA-ZnBr_4$.The ferroelasticity gives potential applications such as optical domain walls memories, optical modulators and tunable active grating for lasers to name a few[20].

$TMA-MnBr_4$ undergoes a second order phase transition at 4 °C[18]. The transition result in a change in structure from orthorhombic structure with the space group *Pmcn* to a monoclinic one with the space group $P_{121/c1}$[18]. The lattice paramters are given in Table 2.1. Tanaka *et al*[18] reports transpartent single crystals with a light yellow green fluorecent color with an external form along the c-axis with psedohexagonal cross section and pyramidal ends.

Table 2.1: Thermodynamic and structure parameters for TMA – $ZnBr_4$ and TMA – $MnBr_4$ including phase transition temperature, space groups, lattice parameters and unit cell volume..

TMA – $ZnBr_4$		TMA – $MnBr_4$	
Phase transition	Space group	Phase transition	Space group
T_c>15°C	Pmcn	T_c>4°C	Pmcn
T_c<15°C	$P12_1/c1$	T_c<4°C	$P12_1/c1$
Lattice parameters[19]		Lattice parameters[22]	
a[Å]	9.238	a[Å]	9.301
b[Å]	16.012	b[Å]	16.182
c[Å]	12.672	c[Å]	12.750
V[Å^3]	1874.4	V[Å^3]	1919

TEA – MBr_4

In the last years several studies have been done on the TEA_2MBr_4 compounds[23]. Wolthuis *et al.*[23] have reported that these crystals have shown several structural phase transitions where some are reported to be ferroelectric. In some cases a second phase transition occur which is followed by a large thermal hysteresis. The TEA cations are, in this type of crystals, disordered at room temperature which implies a possible structural transition at moderate temperatures. The disorder of the cations can originate from fixed β-carbon and a α-carbon with several equivalent stable positions as illustrated for TEA – $ZnBr_4$ in Figure 2.4. This leads to an additional degree of freedom for the TEA cations compared to the TMA cations[23].

Both the organic cation and inorganic anion do have a tetrahedron structure. Ordering the TEA cation in either of the two orientations, as illustrated in Figure 2.4, will reduce the symmetry of the crystal lattice and decrease the volume occupied by the TEA cation. Wolthuis et al.[23] suggests that the free space in the crystal lattice is mainly available for the organic cation and that an increase in the size of the anion will enlarge this further. Simultaneously this will prevent an increase in the steric hindrance of the anion's rotation[12].

Wolthuis *et al.*[23] indicates that when increasing the temperature the motions occuring in the TEA cation will be at first a rotation of the terminal metyl group, secondly, the ethyl group will reorient, thirdly, a reoritentation of the whole molecule around the fourfold inverison axis and at last a reorientation of the whole molecule in all possible ways. Therefore the TEA cations, in A_2MBr_4 at room temperature, are considered to have a rigid structure but with rotation terminal metyl groups[23].

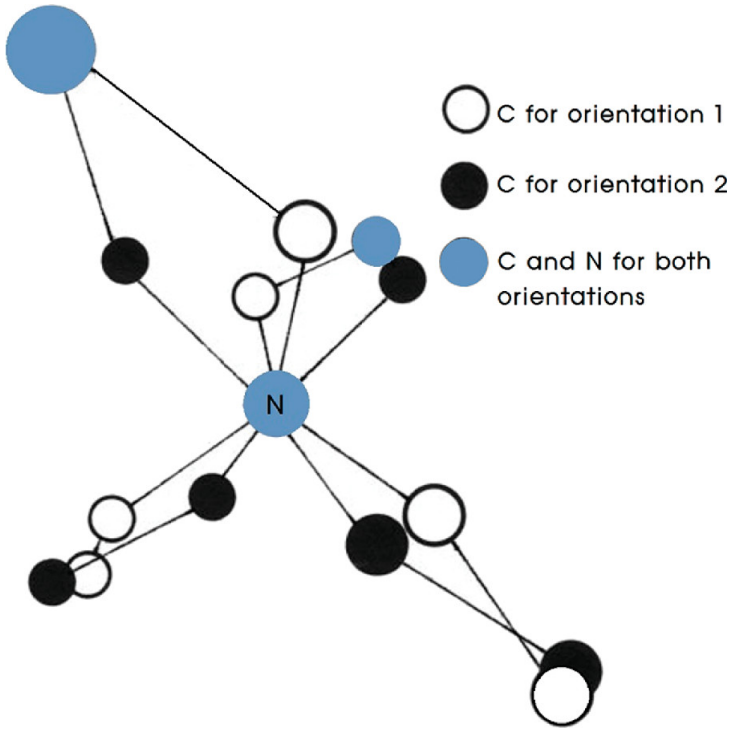

Figure 2.4: The two orientations for the TEA cation in TEA – $ZnBr_4$ where the different orientations of carbon is indicated by white and black balls[12]

For the TEA – $ZnBr_4$ crystals Lim et al. reports two phase transitions on heating. The first one at 10 °C which corresponds to a phase transition and the a second transition at 217 °C corresponding to melting[12]. Lim et al.[12] have observed ferroelastic domains using optical polarizing microscopy at 10 °C. The space group, lattice parameters and unit cell volume at room temperature for TEA – $ZnBr_4$ are given in Table 2.2.

For the TEA – $MnBr_4$ crystals a first-order phase transition is indicated at -13 °C[24]. The space group and lattice paramters are given in Table 2.2.

Table 2.2: Thermodynamic and structure parameters for TEA – $ZnBr_4$ and TEA – $MnBr_4$ including phase transition temperature on heating, space groups, lattice parameters and unit cell volume.

TEA – $ZnBr_4$		TEA – $MnBr_4$	
Phase transition[25]	Space group	Phase transition[26]	Space group
T_c>10°C	$P\bar{4}2_1c$	T_c>-13°C	$P\bar{4}2_1mc$
T_c<10°C	$P1a1$	T_c<-13°C	-
Lattice parameters[25]		Lattice parameters[26]	
a[Å]	8.987	a[Å]	13.203
b[Å]	8.987	b[Å]	13.203
c[Å]	15.977	c[Å]	14.311
V[Å^3]	1290	V[Å^3]	-

TMATEA – MBr_4

Previous research on TMATEA[MBr_4], where M = Zn, Mn, has revealed their convenient physical properties and multiple phase transitions. Figure 2.5 illustrates the TMATEA – $ZnBr_4$ crystal indicating the difference in the two cations present in these molecular structures[27].

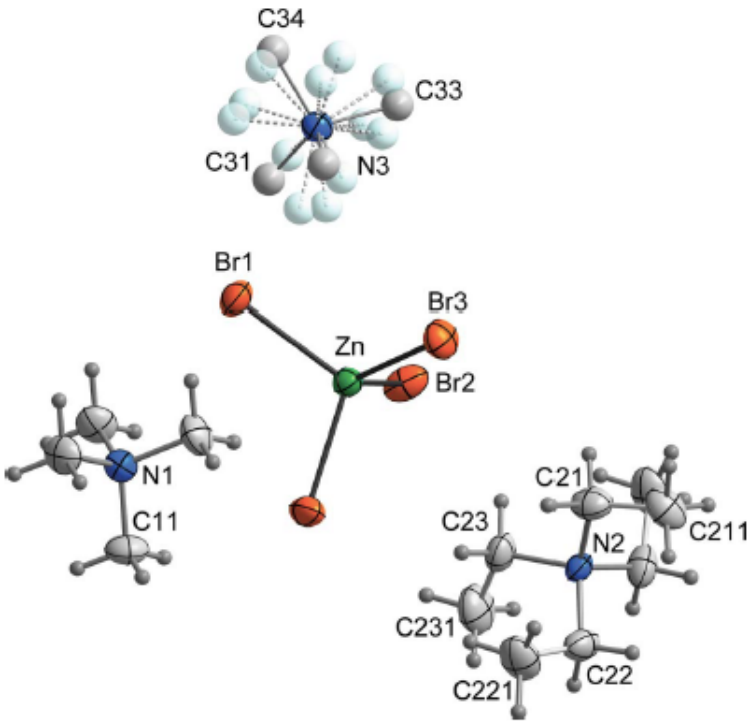

Figure 2.5: The structure of TMATEA – $ZnBr_4$.[27] indicating the different possible orientations in TMA.

In room temperature these crystals have a tetragonal structure. Both the anion, with the atoms Zn, Br1 and Br3 (Figure 2.5) and the TEA-cation, with the atoms N2, C21, C211, C23 and C231, are located in the mirror plane m. The TMA-cation occupies two positions with equal probability where one of the components has site symmertry as illustrated by N1 in Figure 2.5 and the second with symmetry $2mm$ as N3 in Figure 2.5 which is disordered over four equal positions shown as light blue balls in the figure[27].

These crystals have a structure consisting of ions arranged in layers. Two different alternating layers builds up the structure having one with TMA-cations and $[MBr_4]^{2-}$ ions and the second one formed by the TEA-cations.

TMATEA – $ZnBr_4$ undergoes a reversible first-order phase transition with a relatively small temperature hysteresis at 217/ 215 °C on heating and cooling respectively. Krawczyk *et al*[27] reports that the peak from the DSC measurement is indicating a displacive phase transition and the calculated value for the entropy, which is smaller than Rln2, also enhances this indication. However, Krawczyk *et al.* also indicates a pre-transitional effect occuring during the phase transition which is suggested to relate to an increase in dy-

namic disorder. The lattice paramters, space groups and unit cell volume are given in Table 2.3.

TMATEA – $MnBr_4$ undergoes a reversible first-order ferroelastic phase transition at 211/409 °C on heating and cooling run respectively[28]. The phase transition shows the same abnormal behaviour as TMATEA – $ZnBr_4$. The space groups before and after the phase transition, the lattice parameters and the unit cell volume are given in Table 2.3.

Table 2.3: Thermodynamic and structure parameters for TMATEA – $ZnBr_4$ and TMATEA – $MnBr_4$ including phase transition temperature on heating, space groups, lattice parameters and unit cell volume.

TMATEA – $ZnBr_4$		TMATEA – $MnBr_4$	
Phase transition	Space group	Phase transition	Space group
T_c>217°C	$P\bar{4}2_1m$	T_c>211°C	$P\bar{4}2_1m$
T_c<217°C	$P2_12_12$	T_c<211°C	$P2_12_12$
Lattice parameters[27]		Lattice parameters[29]	
a[Å]	13.493	a[Å]	13.622
b[Å]	13.493	b[Å]	13.622
c[Å]	12.030	c[Å]	12.138
V[Å^3]	2190.20	V[Å^3]	2169.65

3 Experimental

Six compositions were made by using the method described in Section 3.1. These crystals were then characterized by X-ray diffraction(XRD) and Differential scanning calorimetry (DSC) as described in Section 3.2. The instruments used in the experimental work are given in Table 3.3.

3.1 Synthesis

Six compositions with the general formula A_2MBr_4 were made using precursors in Table 3.1 by the synthesis method illustrated in Figure 3.1. Which precursors and the amount used is given in Table 3.2. The amount of water used to dissolve the precursors are given in the column to the right for the respective precursor while the water used to fully dilute the mixed solution is given in the column denoted *Mixing H_2O*. To give a better and more detailed insight in the synthesis method the synthesis of TMATEA$-ZnBr_4$ will be described in more detail.

Table 3.1: The precursors used in the synthesis of the compositions with corresponding chemical formula, manufacturer and purity.

Materials	Sample name	Chemical formula	Manufacturer	Purity [%]
Tetramethylammoniumbromide	TMABr	$(CH_3)_4NBr$	Sigma-Aldrich	98
Tetraethylammoniumbromide	TEABr	$(C_2H_5)_4NBr$	Sigma-Aldrich	98
Manganese bromide tetrahydrate		$MnBr_2 \cdot 4\,H_2O$	Sigma-Aldrich	98
Zinc bromide dihydrate		$ZnBr_2 \cdot 2\,H_2O$	Sigma-Aldrich	99

The synthesis of TMATEA$-ZnBr_4$ was carried out by weighing out the precursors zinc bromide dihydrate: $ZnBr_2 \cdot 2\,H_2O$, tetramethylammonium bromide: $(CH_3)_4NBr$ (TMABr) and tetraethylammonium bromide: $(C_2H_5)_4NBr$ (TEABr) (the weight used of each precursor is given in Table 3.2) to achieve a stochiometric ratio of 1:1:1 . The precursors were then dissolved in deionised water and mixed together using a magnetic stirrer (IKA RTC Classic). While mixing more water was added to dissolve the mixed solution. The mixed solution was evaporated slowly in a crystallization dish covered with pin-holed aluminium foil at the bench in the fume hood for 14 days until the most of the excessive water was evaporated. Before characterization of the crystals the more water was removed by vacuum filtration and later in a vacuum oven at 50 °C for 6 hours. The final product of TMATEA$-ZnBr_4$ was then placed in a desiccator.

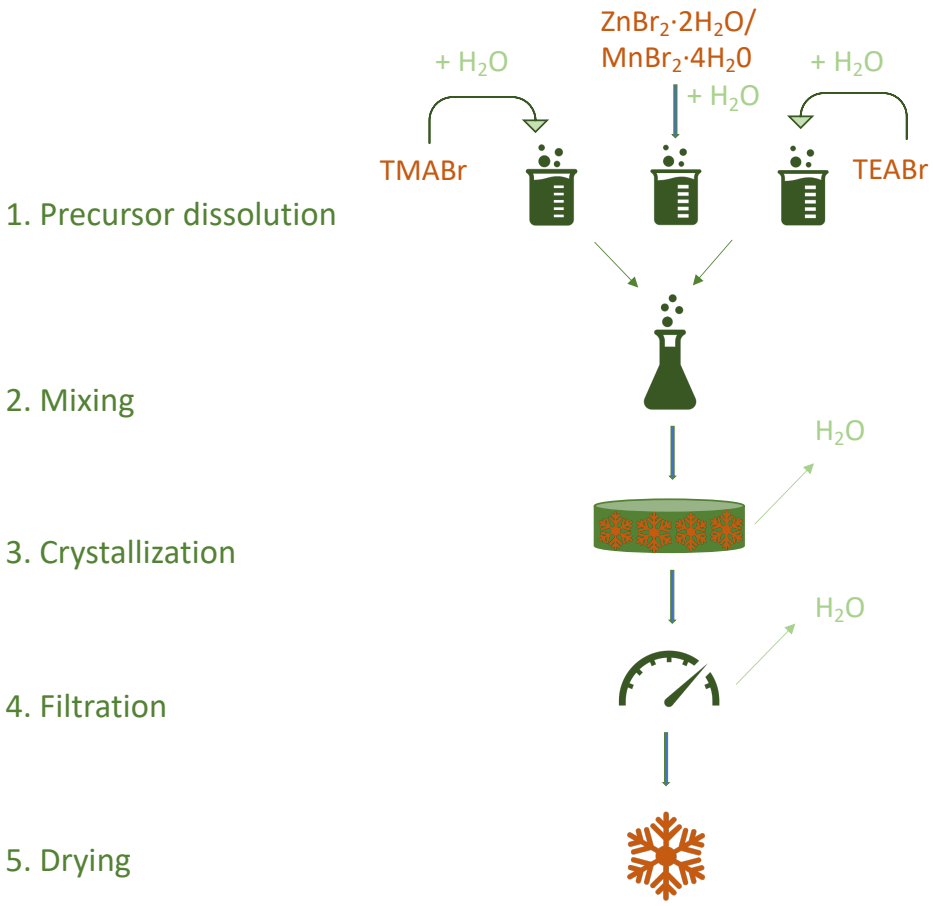

Figure 3.1: Synthesis route for the compositions. The precursors used and the amount is given in Table 3.2.

Table 3.2: Weight of precursors used in the different compounds and amount of water used for dissolving.

	TMABr [g]	H_2O[mL]	TEABr [g]	H_2O [mL]	$ZnBr_2 \cdot 2\,H_2O$[g]	H_2O [mL]	$MnBr_2 \cdot 4\,H_2O$[g]	H_2O [mL]	Mixing H_2O[mL]
TMA–$ZnBr_4$	11.7911	27	-	-	9.8984 g	10	-	-	60
TMA–$MnBr_4$	12.0267	31	-	-	-	-	11.1905	15	10
TMA–TEA–$ZnBr_4$	5.3348	10	7.2748	10	8.9550	10	-	-	74
TMA–TEA–$MnBr_4$	5.4311	10	7.4061	10	-	-	10.1115	20	20
TEA–$ZnBr_4$	-	-	13.2865	20	8.1777	10	-	-	80
TEA–$MnBr_4$	-	-	13.5052	20	-	-	9.2193	25	20

3.2 Characterization

The samples were characterised to determine the structure using XRD and the temperature and enthalpy change of the phase transitions by DSC.

Table 3.3: Instruments used in the project.

Instrument	Model
Scale	Sartorius, METTLER TOLEDO Ag204 Delta Range
XRD	Bruker D8 Focus
Magnetic stirrer/hot plate	IKA RTC Classic
Vacuum drying furnace	Binder VD23
DSC	Netzsch DSC 214 Polyma

3.2.1 XRD

XRD analysis was performed to determine the crystal structure of the samples. The crystals were crushed into a powder with a mortar and filled into a sample holder. The surface of the powder was gently made smooth and flat by sliding a glass plate over the surface. The sample holder was put into D8-Focus X-ray diffractometer. This machine uses CuKα radiation $h\omega$= 8.04 keV, λ= 1.5406 A). All samples were characterised from 10-75 degrees 2θ, for 120 minutes with 0.2 slit-opening. The XRD data was fitted using DIFFRAC.SUITE TOPAS software. First the background was fitted, then crystal L size and the lattice parameters together with a displacment offset. Finally a preferential orientation factor was used. A Cambridge crystallographic data center (CCDC) file was used, for the compounds where it was available, to improve the fit and to make illustrations of the structure in VESTA.

3.2.2 DSC

DSC was used to observe the phase transitions as a function of temperature. Approximately 5 to 10 mg of sample was weighed and placed in a platinum crucible with a lid. The measurements were conducted in a synthetic air gas mixture, with nitrogen safety gas and liquid nitrogen for controlled cooling. The system for measurements was a Netzsch Polyma DSC 214. The crucible and lid are of aluminium. The lid was clamped on top with no hole added (so it was sealed). The temperature program used consisted of three temperature cycles from -25 °C, up to 240 °C and down to -25 °C again. The heating/ cooling rate was set to 10 °C per minute and the holding time at the maximum temperature was 15 minutes.

4 Results

In this chapter the results from the synthesis and characterization of six different crystal compositions are presented. For each composition XRD was used to study the crystal structure with TOPAS and EVA used to identify structural phases and refine crystallographic models to fit the data. DSC was used to study the phase transitions as a function of temperature during both heating and cooling and ascertain the total enthalpy of transition.

4.1 TMA$-ZnBr_4$

The observations of the synthesis, the structural data from XRD measurements and the phase transitions during heating and cooling of TMA$-ZnBr_4$ are presented below.

4.1.1 Observations of synthesis

The tetramethylamminium bromide and the zinc dihydrate bromide solution were clear, also after mixing to the final solution. Small colourless crystals with a hexagonal shape started to grow after 24 hours as shown in Figure 4.1a. After further evaporation of water the crystals obtained the shape and increased in size. The final crystals, Figure 4.1b, were of regular geometric shapes with a narrow size distribution relative to the other compositions, although this was not measured.

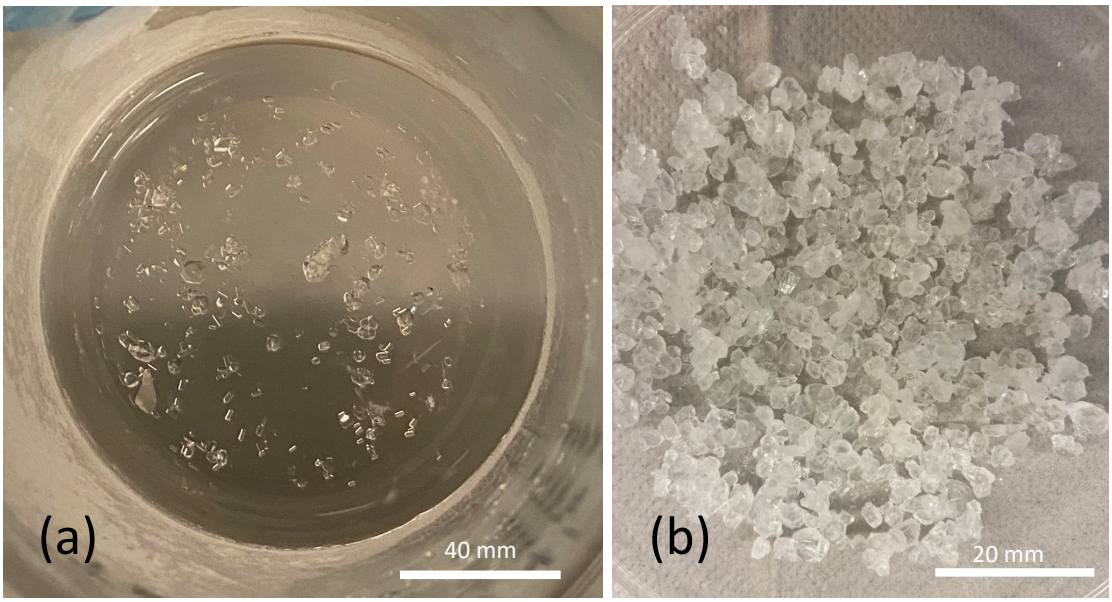

Figure 4.1: Crystal morphology of TMA$-ZnBr_4$ crystals formed by slow evaporation. (a) Initial crystallization and (b) dried product.

4.1.2 Crystal structure

The diffractogram for TMA−$ZnBr_4$ powder is given in Figure 4.2 including the fitted pattern and the difference between these two. The crystallographic information at room temperature for the compound is given in Table 4.1. These values were determined by Rietveld-refinement using TOPAS. The Goodness of fit (GOF) is included in Table 4.1 and is an indication on how well the refinement fits to the diffractogram for observed data of the crushed TMA−$ZnBr_4$ and has a value of 8.04. The structure is determined to have a orthorhombic lattice with space group Pmcn and lattice parameters a=9.255 Å, b=16.055 Å and c=12.691 Å which differ from the data reported by Asahi *et al.*[19] with respectively +0.017, +0.043 and +0.019.

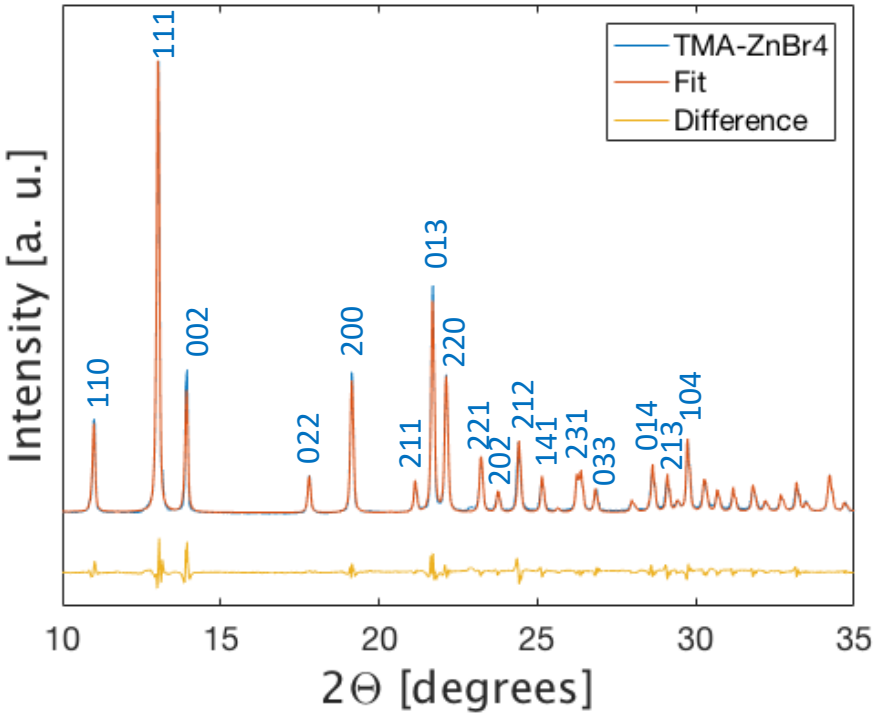

Figure 4.2: Diffractogram for TMA−$ZnBr_4$ powder including the diffractogram for the fit done by Rietveld-refinement and difference between these two. The Miller indices are given on top of the corresponding peak.

Table 4.1: The crystallographic information at room temperature for TMA−$ZnBr_4$.

TMA−$ZnBr_4$	
Temperature [K]	295
Crystal system	Orthorhombic
Space group	Pmcn
a [Å]	9.2551
b [Å]	16.0552
c [Å]	12.6910
V [$Å^3$]	1885.7900
GOF	8.04

A crytallographic information file (CIF) for TMA−$ZnBr_4$ was made using positional parameters reported by Asahi *et al.*[19] which was then used to illustrate the structure in VESTA as one can see in Figure 4.3.

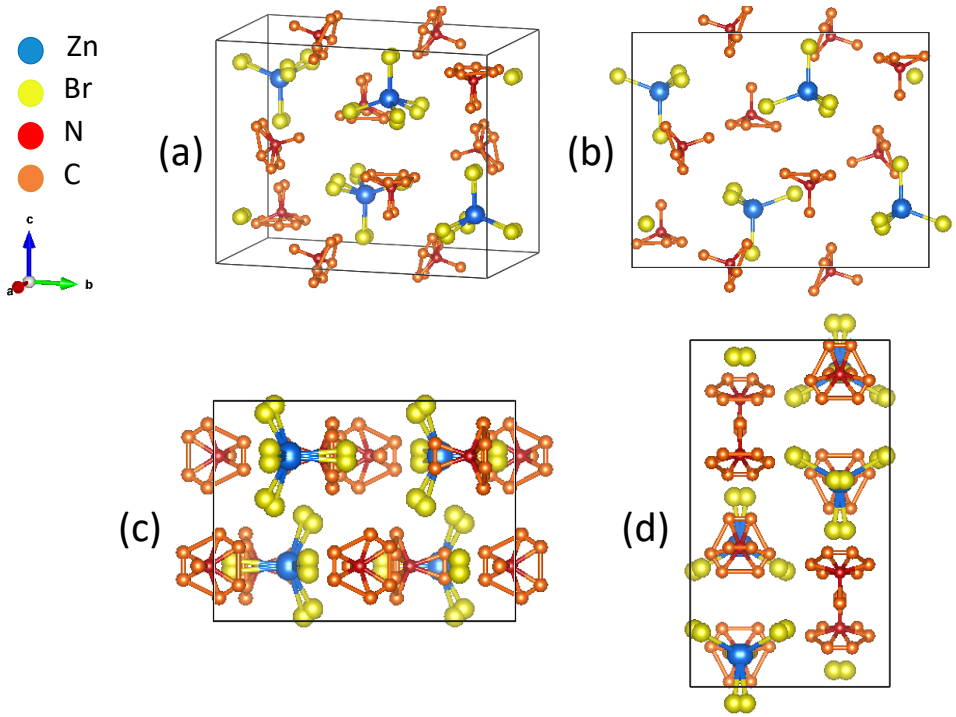

Figure 4.3: Crystal structure for TMA−$ZnBr_4$ illustrated in different directions. (a) shows the standard unit cell aligned according to the axis arrows show. Each additional figure shows a perspective of the structure with a specific axis coming out of the page (b) the A-axis, (c) the B-axis and (d) the C-axis.

In Fig 4.3 (a) The two sublattices of molecular positions, that is for the cation $[N(CH_3)_4]^+$ and anion $[ZnBr_4]^{2-}$. In (b) the anions may be described as having approximate up and down orientations while the cation appears to have six possible orientations and exhibit rotation about a single axis, indicated by the equivalent carbon positions in each molecule occurring around one rotational axis. In (c) the anion and cations form a alternating layered structure with the layers running parallel to the A-direction. In (d) the single axis of rotation for each organic molecule can be more easily seen and the variation in the orientation of that axis through out the different sites in the crystal lattice.

4.1.3 Phase transitions

To determine the thermal behaviour of the compound a DSC measurement was performed during heating and cooling from -25 °C to 240 °C for three cycles. A reversible phase transition occur at 7°C and 15 °C on heating and cooling respectively with a temperature hysteresis of 8 °C which is quite consistent with values reported by Kirachi[20]. The transition peak is asymmetric and do have a diffuse characteristic on the lower temperature side while a sharp one on the high temperature side. Under these heating and cooling conditions the transition is reversible and repeatable. The peak around -20 °C is an artefact from the measurement and is therefore not studied further.

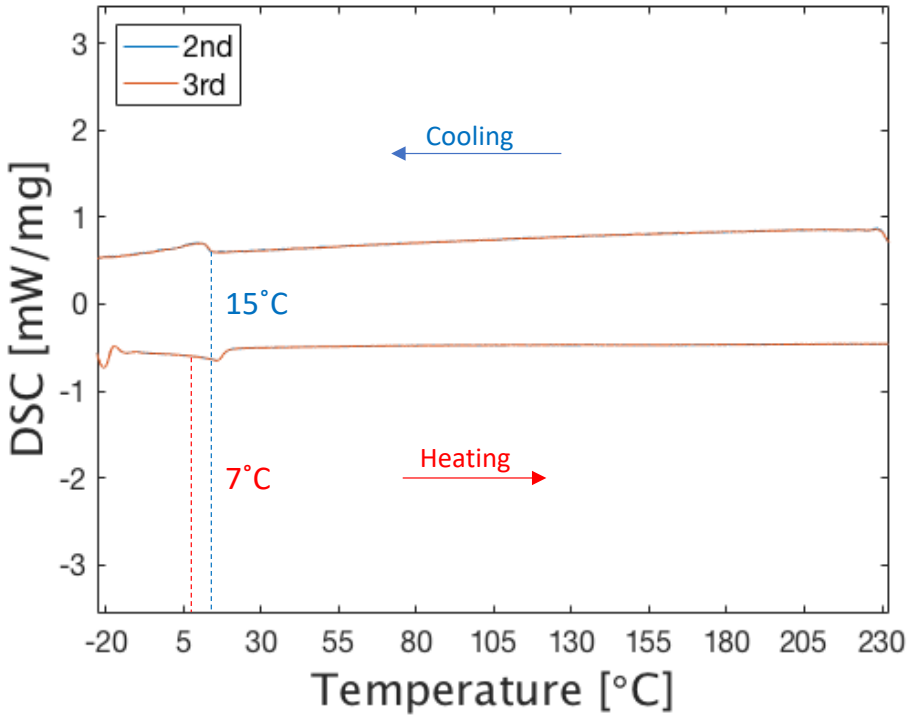

Figure 4.4: DSC results for TMA$-ZnBr_4$ crystals. The sample was cycled between -25 °C and 240 °C three times (the fist cycle is not included). The phase transitions are marked with red and blue dotted lines for heating and cooling respectively.

The enthalpy of transition, H_{fus}, indicate the amount of energy each transition releases or absorbs. Using Figure 4.4 H_{fus} is determined by calculating the area under the corresponding peak. These values,the enthalpy of transition,H_{fus}, is given in Table 4.2.

Table 4.2: H_{fus} for the phase transitions occurring in TMA – $ZnBr_4$ on heating and cooling.

T [°C]	H_{fus} [J/g]
7	12.4
15	18.86

4.2 TMA – $MnBr_4$

The observations of the synthesis, the structural data from XRD measurements and the phase transitions during heating and cooling of TMA – $MnBr_4$ are presented below.

4.2.1 Observations of synthesis

After 24 hours the growth of needle-like pinkish transparent crystals had started as shown in Figure 4.5a. The presence of small particles precipitated from the solution and the color segregation in Figure 4.5b suggests that there is some chemical segregation. After further slow evaporation the crystals got a dendritic structure while the color was slightly changed to a pinksih solution and yellow crystals (Figure 4.5b). After filtration and drying the crystals were all yellow as shown in Figure 4.5c.

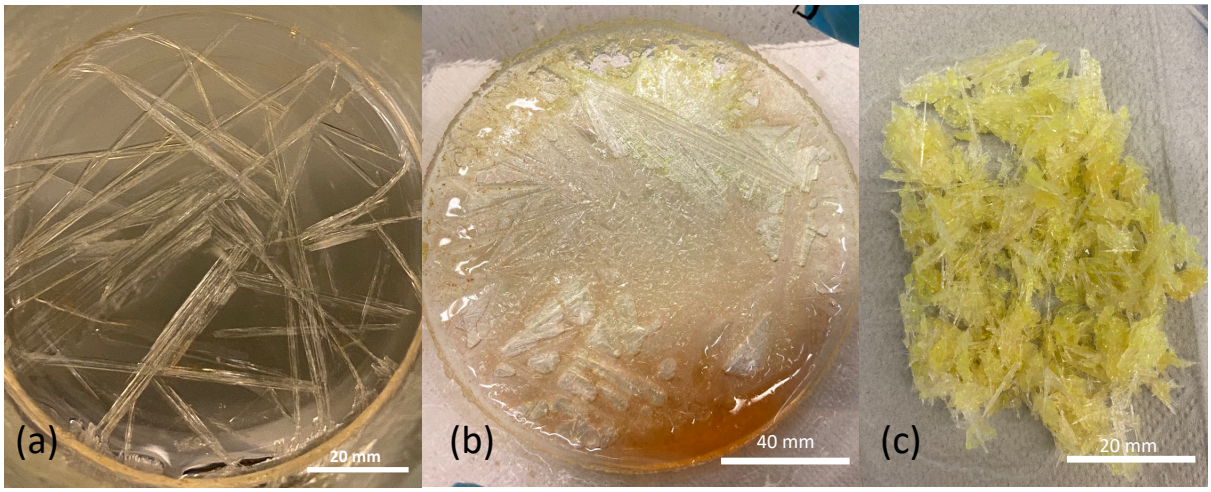

Figure 4.5: Crystal morphology of TMA – $MnBr_4$ crystals formed by slow evaporation. (a) Initial crystallization after 24 hours, (b) after two weeks of slow evaporation (c) dried product.

4.2.2 Crystal structure

The diffractogram for TMA−$MnBr_4$ powder is given in Figure 4.6 including the fitted pattern and the difference between these two. The crystallographic information at room temperature for the compound is given in Table 4.3. These values were determined by Rietveld-refinement using TOPAS. The Goodness of fit (GOF) is included in the Table 4.3 and is an indication on how well the refinement fits to the diffractogram for observed data of the crushed TMA−$MnBr_4$ and has a value of 10.32. The structure was determined to have a orthorhombic lattice with space group Pmcn and lattice parameters a=9.2960 Å, b=16.200 Å and c=12.7468 Å which differ from values reported by Ashai *et al*[22] by respectively -0.005, +0.018 and -0.003.

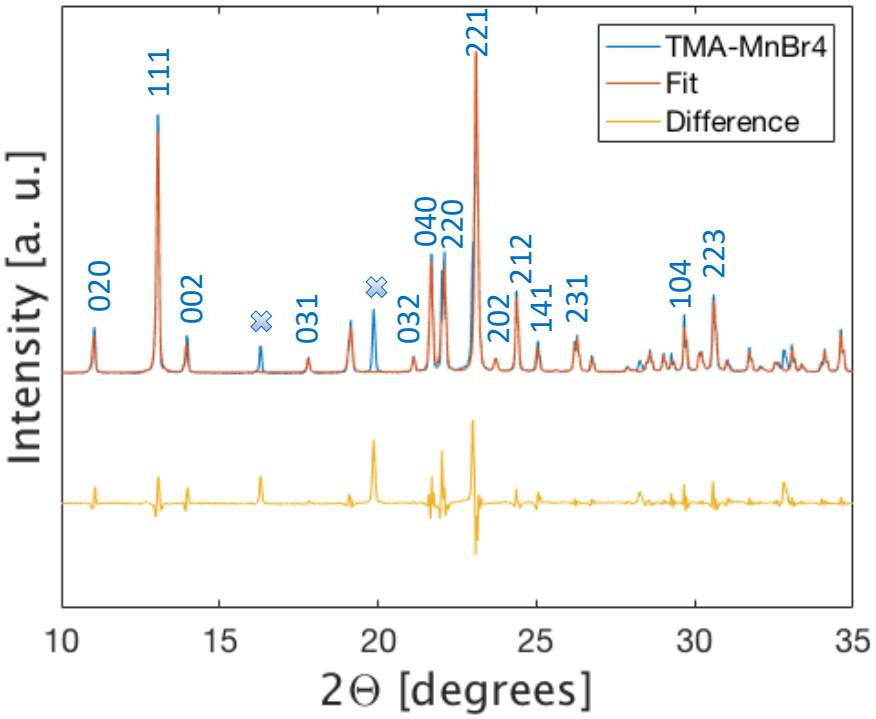

Figure 4.6: Diffractogram for TMA−$MnBr_4$ powder including the diffractogram for the fit done by Rietveld-refinement and difference between these two. The Miller indices are given on top of the corresponding peak. Two of the main peaks, marked with a cross, belongs to tetramethylammonium bromide (one of the precursors).

Table 4.3: The crystallographic information at room temperature for TMA – $MnBr_4$.

TMA – $MnBr_4$	
Temperature [K]	295
Crystal system	Orthorhombic
Space group	Pmcn
a [Å]	9.2960
b [Å]	16.1999
c [Å]	12.7468
V [$Å^3$]	1919.6036
GOF	10.32

A crytallographic information file (CIF) for TMA – $ZnBr_4$ was made using positional parameters reported by Asahi *et al.*[19] and then modified to fit TMA – $MnBr_4$ and then used to illustrate the structure in VESTA as one can see in Figure 4.7.

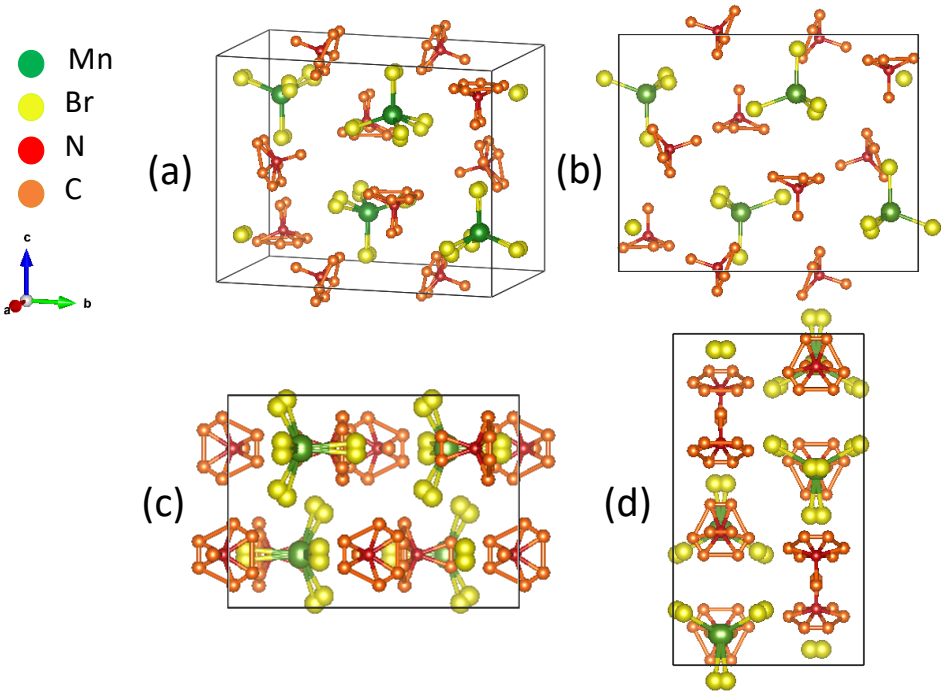

Figure 4.7: Crystal structure for TMA – $MnBr_4$ illustrated in different directions. (a) shows the standard unit cell aligned according to the axis arrows show. Each additional figure shows a perspective of the structure with a specific axis coming out of the page (b) the A-axis, (c) the B-axis and (d) the C-axis.

The structure for TMA – $MnBr_4$ is similar to the one described for TMA – $ZnBr_4$ in section

4.1.2 except for the anion which is $[MnBr_4]^{2-}$ for this structure.

4.2.3 Phase transitions

To determine the thermal behaviour of the compound DSC measurements was performed during heating and cooling from -25 °C to 240 °C for three cycles. A reversible phase transition occur at 0 °C and 5 °C during heating and cooling respectively with a relatively small temperature hysteresis of 5 °C which is consistent of what is reported by Tanaka *et al.*[18]. The peak do have a diffuse characteristic at the lower temperature side while a sharper shape at the higher temperature side. Peaks appearing at -20 °C and 230 °C are measurement artefacts and are therefore neglected in further analysis.

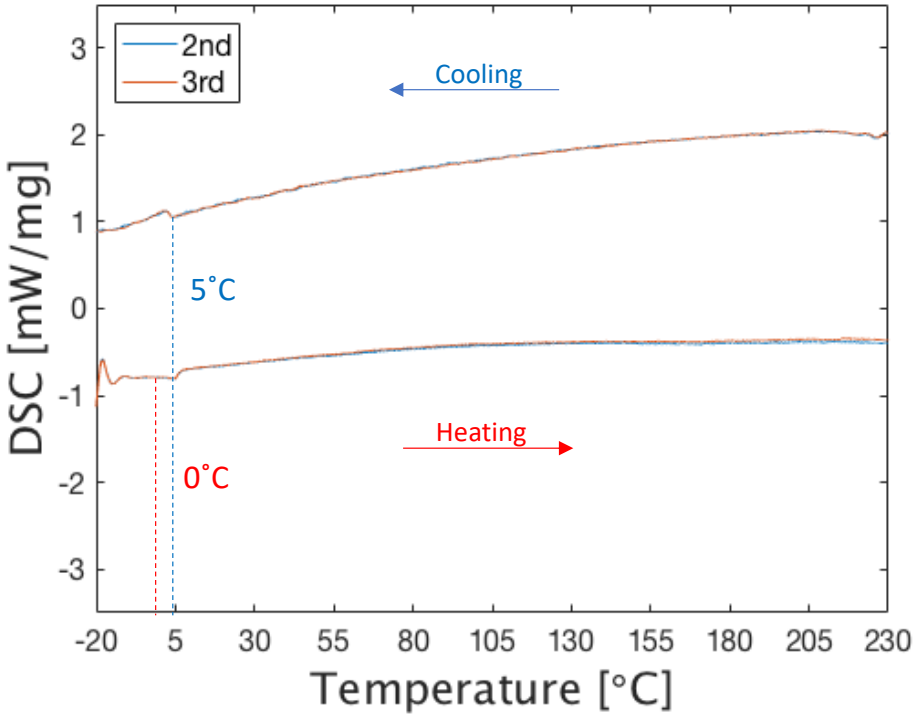

Figure 4.8: DSC results for TMA−$MnBr_4$ crystals. The sample was cycled between -25 °C and 240 °C three times (the fist cycle is not included). The phase transitions are marked with red and blue dotted lines for heating and cooling respectively.

The enthalpy of transition, H_{fus}, indicate the amount of energy each transition releases or absorbs. Using Figure 4.8 H_{fus} is determined by calculating the area under the corresponding peak. These values,the enthalpy of transition,H_{fus}, is given in Table 4.4.

Table 4.4: H_{fus} for the phase transitions occurring in TMA−$MnBr_4$ on heating and cooling.

T [°C]	H_{fus} [J/g]
0	7.071
5	10.67

4.3 TEA – $ZnBr_4$

The observations of the synthesis, the structural data from XRD measurements and the phase transitions during heating and cooling of TEA – $ZnBr_4$ are presented below.

4.3.1 Observations of synthesis

For TEA – $ZnBr_4$ both the precursor solutions, TEABr and zinc bromide dihydrate, were clear both before and after mixing to the final solution. After five days of slow evaporation of water the crystal growth started. As one can see in Figure 4.9a the first precipitation of crystals was a mix of agglomerates of smaller crystals and bigger single crystals. The single crystals, shown in Figure 4.9c, were squares of a size about 4 cm^2 and 2 mm thick. The crystallization steps are visible in Figure 4.9c in diagonal, verticle and horizontal direction . However the rest of the final product, FigureXXb, was smaller powder-like crystals.

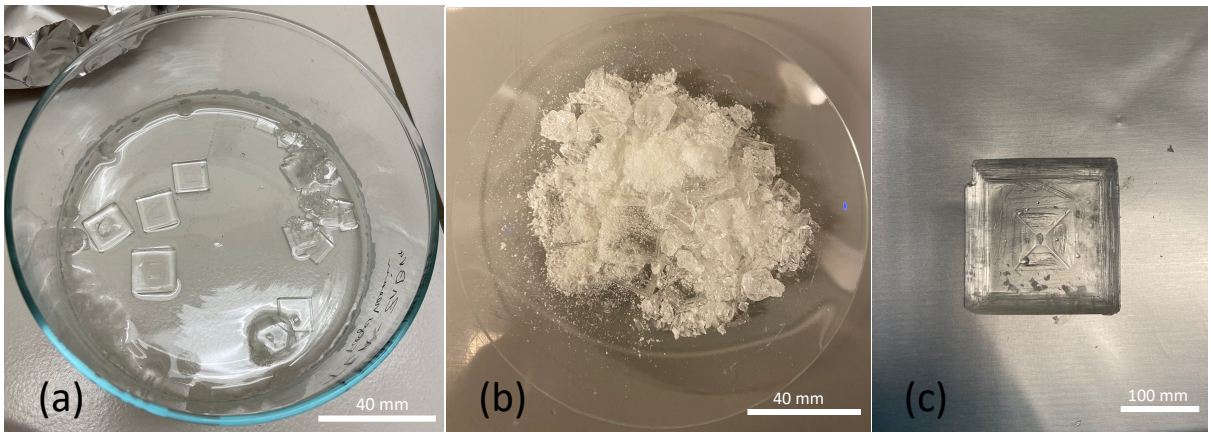

Figure 4.9: Crystal morphology of TEA – $ZnBr_4$ crystals formed by slow evaporation. (a) Initial crystallization, (b) dried product and (c) single crystal.

4.3.2 Crystal structure

The crystal structure was determined at room temperature by performing XRD and Rietveld-refinement using TOPAS. The diffractogram for TEA – $ZnBr_4$ powder is given in Figure 4.10 including the fitted pattern and the difference between these two. The Miller indices are given on top of the corresponding peak.

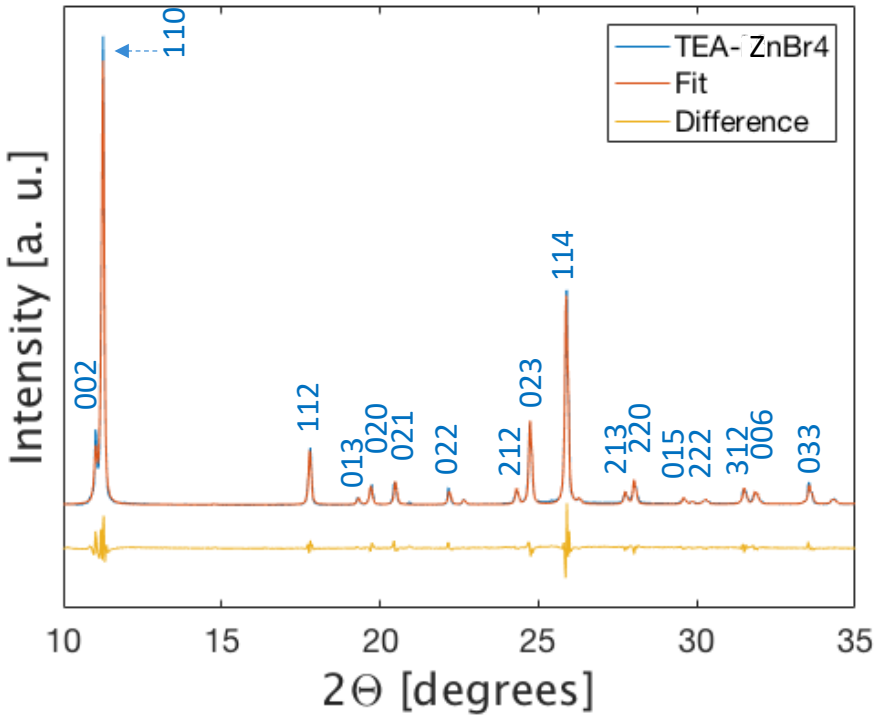

Figure 4.10: Diffractogram of TEA – $ZnBr_4$ powder including the diffractogram for the fit done by Rietveld-refinement and difference between these two. The Miller indices are given on top of the corresponding peak.

The crystallographic information at room temperature for the compound is given in Table 4.5. These values were determined by Rietveld-refinement using TOPAS. The Goodness of fit (GOF) is included in the Table XX and is an indication on how well the refinement fits to the diffractogram for observed data of the crushed TEA – $ZnBr_4$ and has a value of 6.32. The structure is determined to have a tetragonal lattice with space group $P\bar{4}2_1c$ and lattice parameters a=b=8.996 Å and c=16.008 Å which differs from the data reported by Sondergeld *et al.*[25] with respectively +0.008 and +0.031.

Table 4.5: The crystallographic information at room temperature for TEA – $ZnBr_4$.

TEA – $ZnBr_4$	
Temperature [K]	295
Crystal system	Tetragonal
Space group	$P\bar{4}2_1c$
a [Å]	8.996
b [Å]	8.996
c [Å]	16.008
V [$Å^3$]	1295.353
GOF	6.32

A crytallographic information file (CIF) for TEA – $ZnBr_4$ was made by using the structural data and the TOPAS fit. Using VESTA the CIF was used to illustrate the structure as one can see in Figure 4.11.

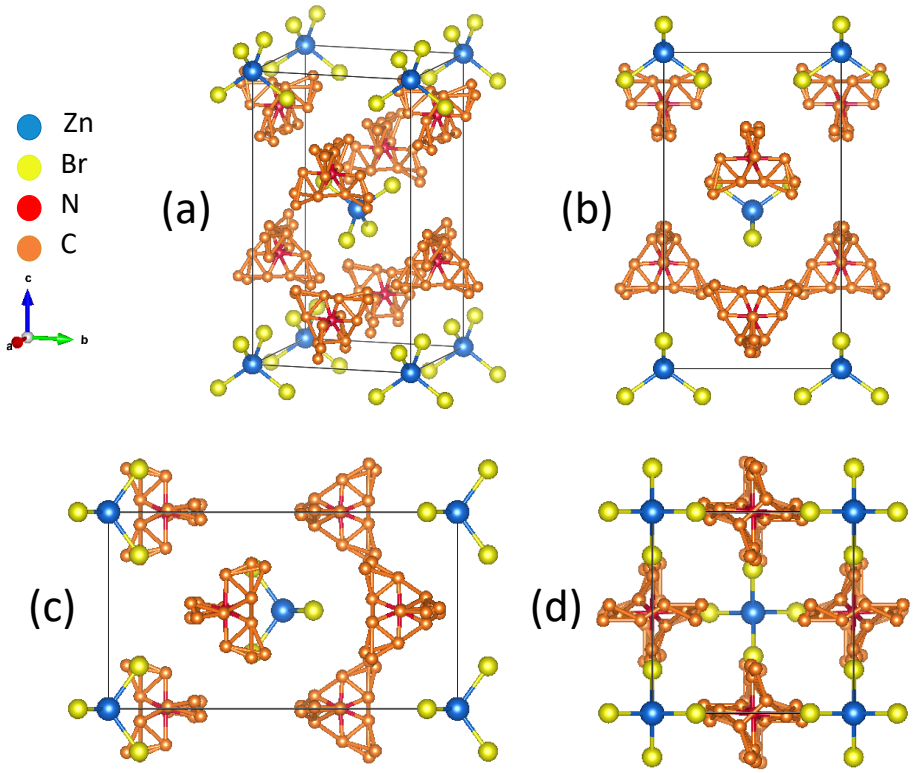

Figure 4.11: Crystal structure for TEA – $ZnBr_4$ illustrated in different directions. (a) shows the standard unit cell aligned according to the axis arrows show. Each additional figure shows a perspective of the structure with a specific axis coming out of the page (b) the A-axis, (c) the B-axis and (d) the C-axis.

In Figure 4.11a the unit cell clear shows two sublattices of the anion and cation positions. The anions occupy the corners and body center positions of the unit cell. In (b) the cations can be seen to form two approximate planes though the structure perpendicular to, and at the approximate 1/4 and 3/4, of C-axis heights through the structure. The specific axis of rotation of the individual molecules is difficult to identify. In (c) similar structural features as are visible and in (d) it is possible to see that the cations occupy the middle of each side of the unit cell when the C-axis is directed out of the page.

4.3.3 Phase transitions

To determine the thermal behaviour of the compound a three cycled DSC measurement was performed from -25 °C to 240 °C. Two reversible phase transitions occur as one can see in Figure 4.12. The first one at 10 °C with minimal hysteresis in the transition temperature between heating and cooling and the second one at 220 °C and 190 °C during heating and cooling respectively with a moderate hysteresis resulting in a temperature

difference of 30 °C. The phase transition temperatures are consistent with previously reported values[23].The peak around 230 °C is an artefact from the measurement and is therefore not studied further.

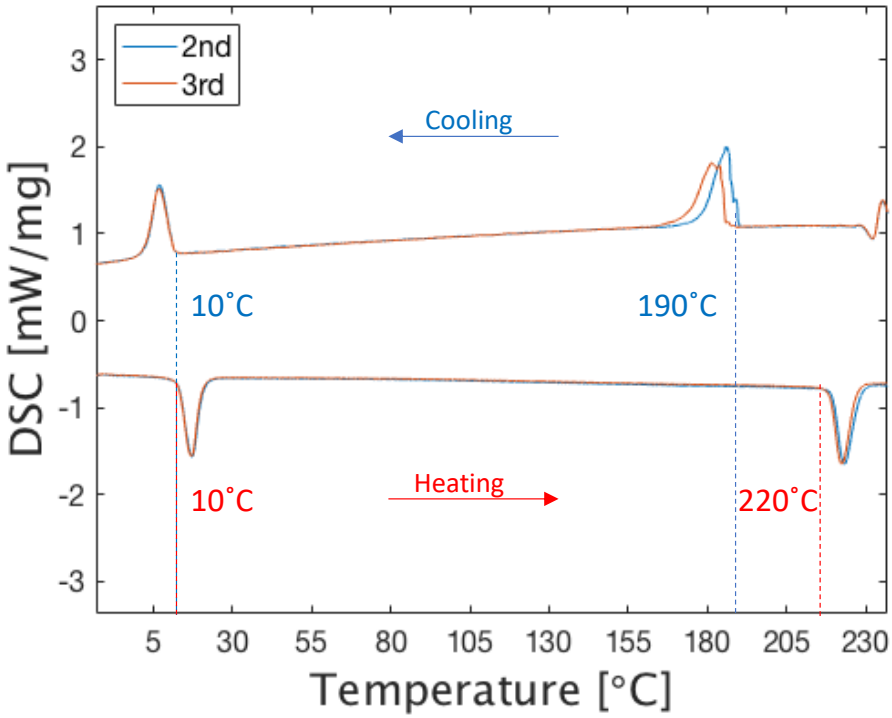

Figure 4.12: DSC results for TEA$-ZnBr_4$ crystals. The sample was cycled between -25 °C and 240 °C three times (the fist cycle is not included). The phase transitions are marked with red and blue dotted lines for heating and cooling respectively.

The first transition possess peaks that are sharp and symmetrical, meaning the transition is likely first order. The peak for the second transition is symmetrical on heating but have some deviation on cooling, it also changes between second and third cycle on cooling. As the other peaks are all identical between cycles it is unlikely that there is some non-reversible change occurring. The transition peaks on cooling of plastic crystals are known to be unstable and shift erratically, hence it is indicated that a large entropy change is taking place that is related to the molecular rotation.

The enthalpy of transition, H_{fus}, indicate the amount of energy each transition releases or absorbs. Using Figure 4.12 H_{fus} is determined by calculating the area under the corresponding peak. These values, the enthalpy of transition,H_{fus}, is given in Table 4.6.

Table 4.6: H_{fus} for the phase transitions occurring in TEA – $ZnBr_4$ on heating and cooling.

Transition	T [°C]	H_{fus} [J/g]
1	10	26.38
	10	26.11
2	220	30.42
	190	41.14

4.4 TEA – $MnBr_4$

The observations of the crystal growth, the structural data from XRD measurements and the phase transitions during heating and cooling found by DSC measurements of TEA – $MnBr_4$ are presented below.

4.4.1 Observations of synthesis

The tetraethylamminium bromide solution was clear while the manganese bromide tetrahydrate solution had a pinkish colour. When mixing the two precursor solutions it retained the slightly pink colour. After ten days of slow evaporation of water the initial crystal growth was observed. As one can see in Figure 4.13a the first precipitation of crystals was a mix of yellow agglomerates and bigger single crystals while the solution retained the pinkish colour. The single crystals had both hexagonal and square-like shapes and various sizes. The dried product (Figure 4.13b) was yellow and the crystals still had a mixture of irregular shapes and sizes of around 1 cm^2 and thickness of 2 mm.

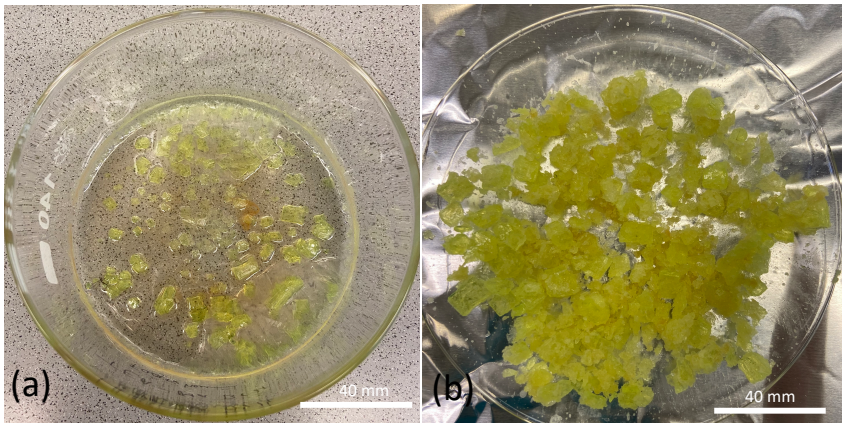

Figure 4.13: Crystal morphology of TEA – $MnBr_4$ crystals formed by slow evaporation. (a) Initial crystallization, (b) dried product.

4.4.2 Crystal structure

The diffractogram for TEA – $MnBr_4$ powder is given in Figure 4.14 including the fitted pattern and the difference between these two.

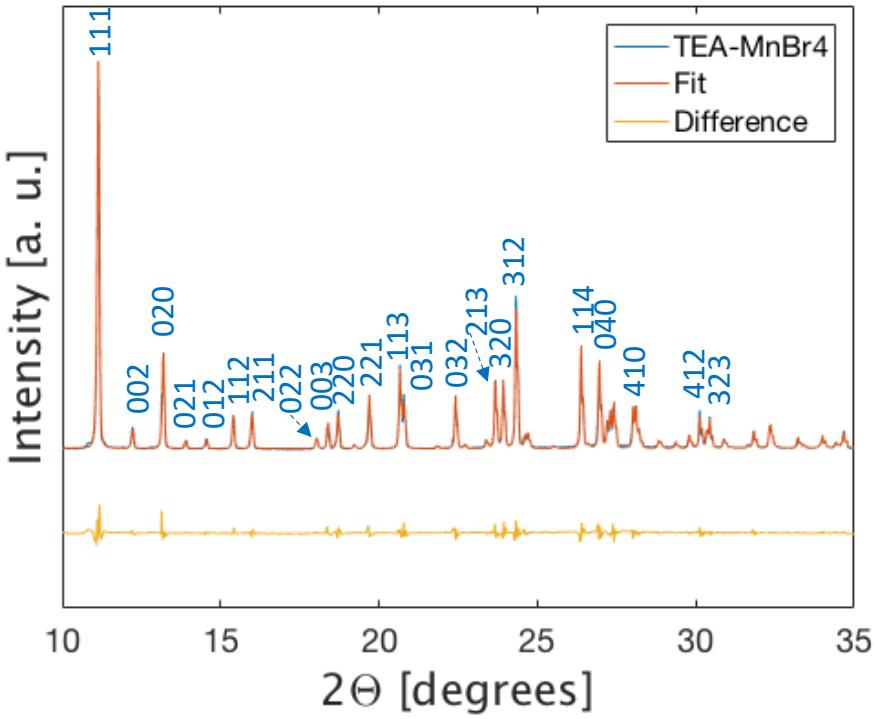

Figure 4.14: Diffractogram for TEA – $MnBr_4$ including the diffractogram for the fit done by Rietveld-refinement and difference between these two. The Miller indices are given on top of the corresponding peak.

The crystallographic information at room temperature for the compound is given in Table 4.7. These values were determined by Rietveld-refinement using TOPAS. The Goodness of fit (GOF) is included in the Table 4.7 and is an indication on how well the refinement fits to the diffractogram for observed data of the crushed TEA – $MnBr_4$ and has a value of 3.89. The structure was determined to have a tetragonal lattice with space group $P\bar{4}2_1m$ and lattice parameters a=b=13.393 Å and c=14.444 Å which differ from the data reported by Chen *et al.*[26] with respectively +0.191 and +0.133.

Table 4.7: The crystallographic information at room temperature for TEA – $MnBr_4$.

TEA – $MnBr_4$	
Temperature [K]	295
Crystal system	Tetragonal
Space group	$P\bar{4}2_1m$
a [Å]	13.393
b [Å]	13.393
c [Å]	14.444
V [Å^3]	2590.687
GOF	3.89

A crytallographic information file (CIF) for TEA – $MnBr_4$ [30] was used to illustrate the structure in VESTA as one can see in Figure 4.15.

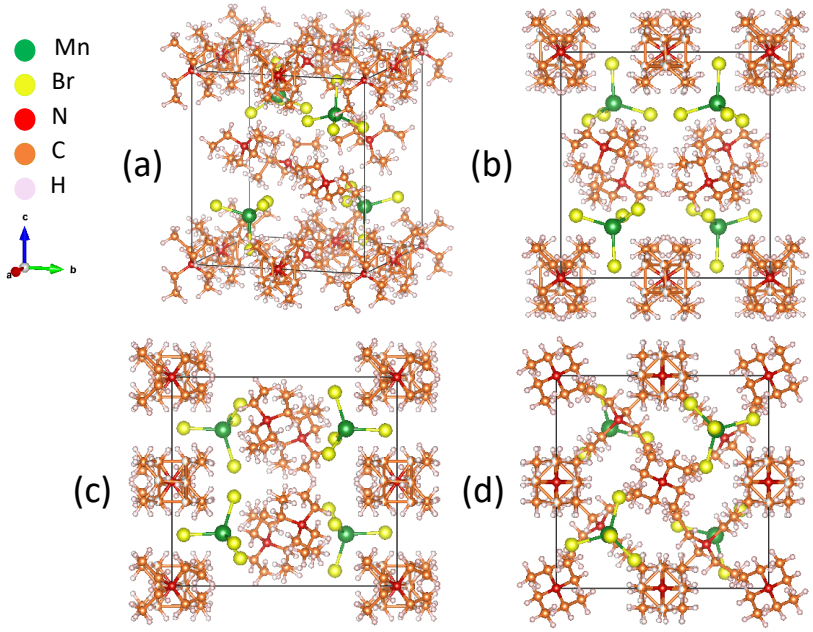

Figure 4.15: Crystal structure for TEA – $MnBr_4$ illustrated in different directions. (a) shows the standard unit cell aligned according to the axis arrows show. Each additional figure shows a perspective of the structure with a specific axis coming out of the page (b) the A-axis, (c) the B-axis and (d) the C-axis.

The layered structure has alternating organic-inorganic sublattices in the A- and C-direction. The $[N(C_2H_5)_4]+$ cations has two different stable confirmations which both present in Figure 4.15. The anion sublattice occupies the approximate center of each of for quadrants of the unit cell and are located between the cation sublattices.

4.4.3 Phase transitions

To determine the thermal behaviour of the compound DSC measurements was performed during heating and cooling from -25 °C to 240 °C for three cycles. The first transition at -15 °C and -5 °C during heating and cooling respectively with a temperature hysterisis of 10 °C and the second transition at 160 °C and 125 °C during heating and cooling respectively with a hysterisis of 35 °C. The peak at around 125 °C shifts for the second and third cycle on cooling. The peak for the third cycle shifts towards lower temperatures and do appear to have a shoulder. It is suggested that the phase transitions are reversible as all the other peaks are identical. The peak around -20 °C on heating is an artefact which originates from the measurement and not the sample and is therefore neglected from the further analysis.

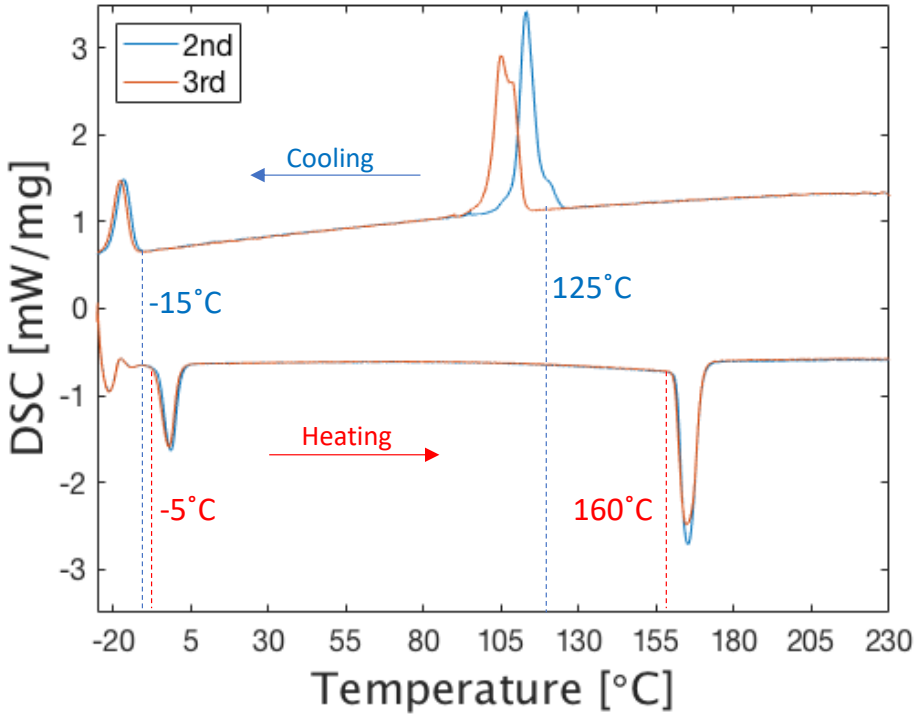

Figure 4.16: DSC results for TEA−$MnBr_4$ crystals. The sample was cycled between -25 °C and 240 °C three times (the fist cycle is not included). The phase transitions are marked with red and blue dotted lines for heating and cooling respectively.

The enthalpy of transition, H_{fus}, indicate the amount of energy each transition releases or absorbs. Using Figure 4.16 H_{fus} is determined by calculating the area under the corresponding peak. These values,the enthalpy of transition,H_{fus}, is given in Table 4.8.

Table 4.8: H_{fus} for the phase transitions occurring in TEA−$MnBr_4$ on heating and cooling.

Transition	T [°C]	H_{fus} [J/g]
1	-5	26.3
	-15	27.62
2	160	70.01
	125	87.33

4.5 TMATEA−$ZnBr_4$

4.5.1 Observations of synthesis

All the precursor solutions (tetramethylammonium bromide, tetraethylammonium bromide and zinc bromide dihydrate) were clear both before and after mixing the final solution. As one can see in Figure 4.17a the first participation of crystals were small

hexagonal shaped single crystals. As more water slowly evaporated the single crystals agglomerated as seen in Figure 4.17b. The size and shape distribution is limited.

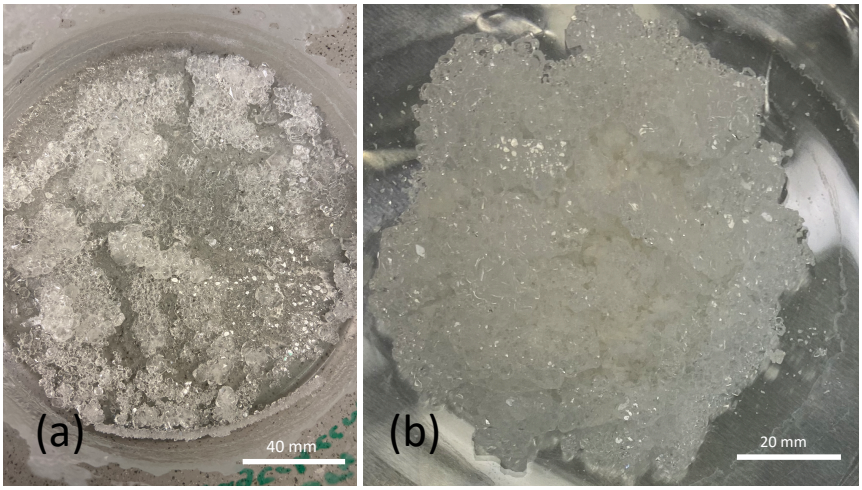

Figure 4.17: Crystal morphology of TMATEA – $ZnBr_4$ crystals formed by slow evaporation. (a) Initial crystallization, (b) dried product.

4.5.2 Crystal structure

The diffractogram for TMATEA – $ZnBr_4$ powder is given in Figure 4.18 including the fitted pattern and the difference between these two. The crystallographic information at room temperature for the compound is given in Table 4.9. These values were determined by Rietveld-refinement using TOPAS. The Goodness of fit (GOF) is included in the Table XX and is an indication on how well the refinement fits to the diffractogram for observed data of the crushed TMATEA – $ZnBr_4$ and has a value of 6.78. The structure is determined to have a tetragonal lattice with space group P21m and lattice parameters a=b=13.552 and c=12.083 with a difference of respectively +0.059 and +0.053 from the values reported by Krawczyk *et al.*[27].

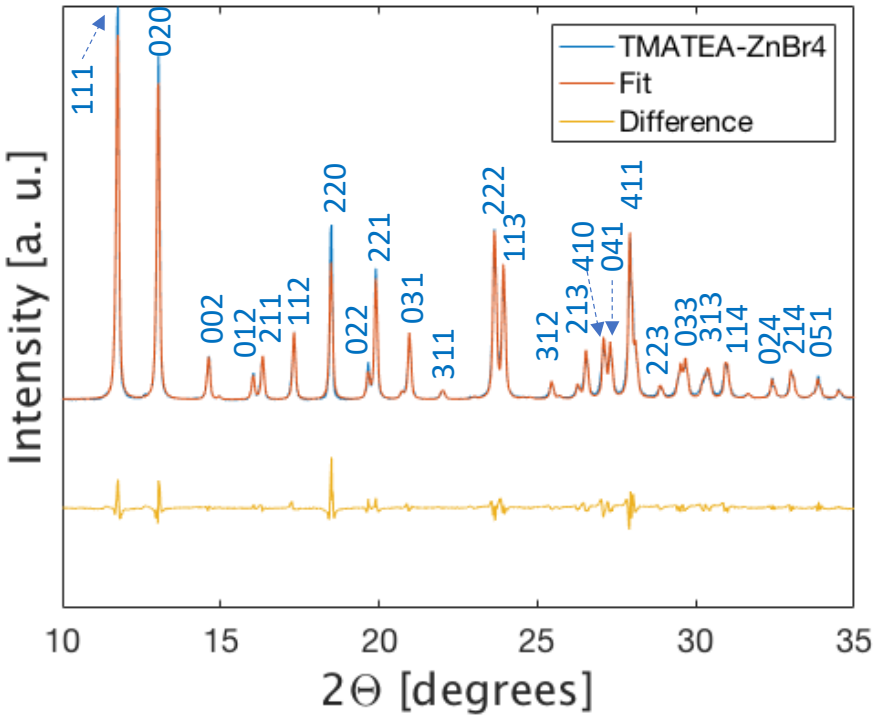

Figure 4.18: Diffractogram for TMATEA$-ZnBr_4$ powder including the diffractogram for the fit done by Rietveld-refinement and difference between these two. The Miller indices are given on top of the corresponding peak.

Table 4.9: The crystallographic information at room temperature for TMATEA$-ZnBr_4$.

TMATEA$-ZnBr_4$	
Temperature [K]	295
Crystal system	Tetragonal
Space group	$P\bar{4}21m$
a [Å]	13.5521
b [Å]	13.5521
c [Å]	12.0834
V [Å^3]	2219.2360
GOF	6.78

A crytallographic information file (CIF) for TMATEA$-ZnBr_4$ was used to illustrate the structure in VESTA as one can see in Figure 4.19.

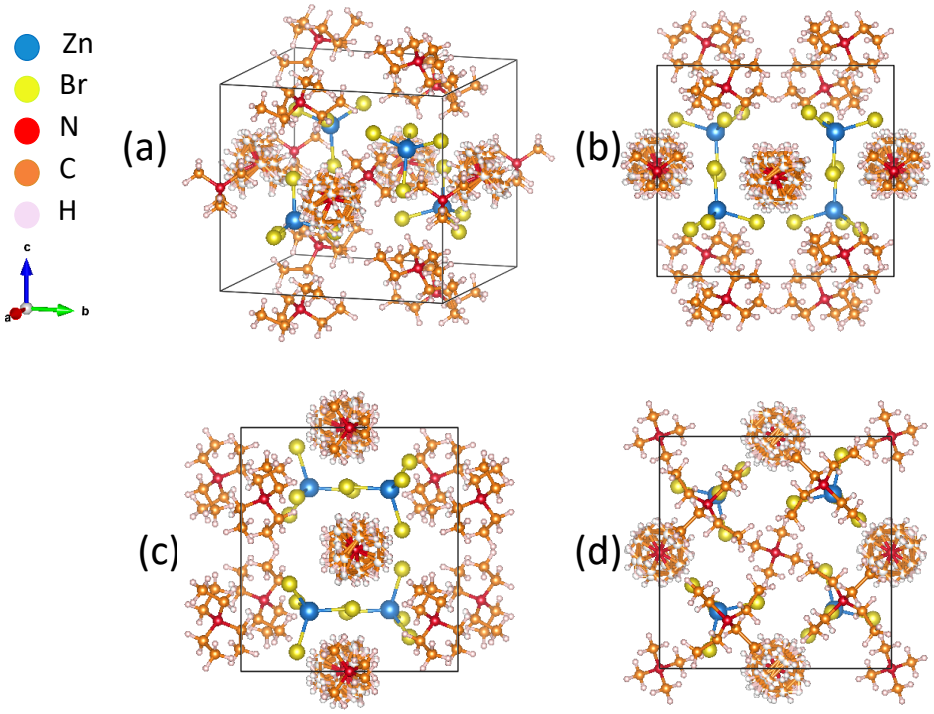

Figure 4.19: Crystal structure for TMATEA – $ZnBr_4$ illustrated in different directions. (a) shows the standard unit cell aligned according to the axis arrows show. Each additional figure shows a perspective of the structure with a specific axis coming out of the page (b) the A-axis, (c) the B-axis and (d) the C-axis..

Two cation sublattices are present in this structure, $[N(C_2H_5)_4]^+$ and $[N(CH_3)_4]^+$, which are layered alternating with the anion lattice $ZnBr_4{}^{2-}$ between the layers, as one can see in Figure 4.19b and 4.19c. The $[N(CH_3)_4]^+$ do occupy a smaller area than the other cation and have more equivalent orientations giving it more degree of rotational freedom [20].

4.5.3 Phase transitions

To determine the thermal behaviour of the compound DSC measurements was performed during heating and cooling from -25 °C to 240 °C for three cycles. A reversible phase transition occur at 215 °C and 217 °C during heating and cooling respectively with a relatively small temperature hysteresis of 2 °C as also reported by Krawczyk *et al.*[27]. The nature of the peak is first an increase starting around 180 °C before the main peak appear at 215 °C and 217 °C indicating the presence of two different reactions. The peak around -20 °C is an artefact due to the transition between heating and cooling and this one is therefore not studied further.

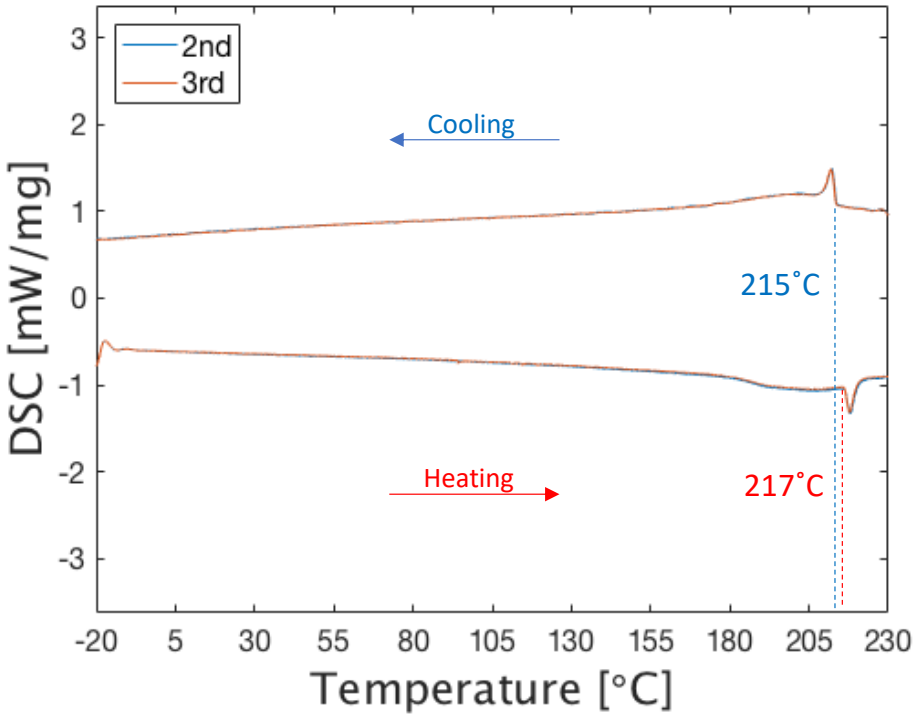

Figure 4.20: DSC results for TMATEA$-ZnBr_4$ crystals. The sample was cycled between -25 °C and 240 °C three times (the fist cycle is not included). The phase transitions are marked with red and blue dotted lines for heating and cooling respectively.

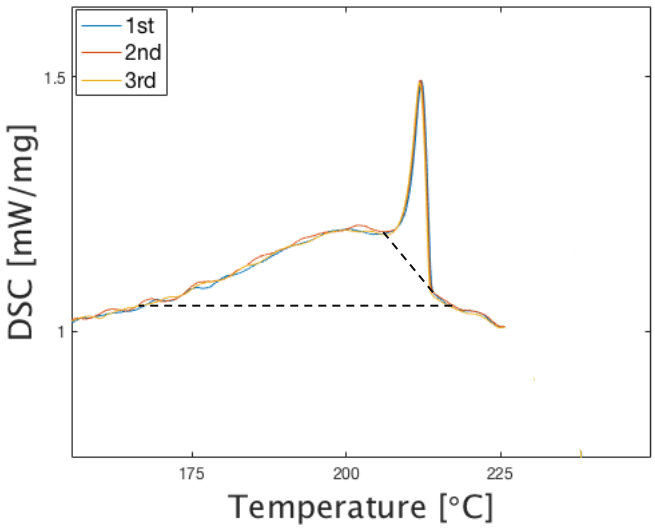

Figure 4.21: An enlarged figure of the DSC-peak at cooling for TMATEA – $ZnBr_4$ with dotted lines that indicates how the enthalpy is determined.

In Figure 4.21 some additional contribution to the heat flow below the phase transition temperature. Szklarz *et al.*[28] reports that these changes of the heat flow indicate significant pre-transitional contribution to the heat capacity and entropy that can be connected with increasing disorder related to the ionic dynamics in the crystal lattice. The enthalpy of transition, H_{fus}, indicate the amount of energy each transition releases or absorbs. Using Figure 4.20 H_{fus} is determined by calculating the area under the corresponding peak and the dependency of the normal part of the heat flow was approximated by the dotted line in Figure 4.21. These values,the enthalpy of transition,H_{fus}, is given in Table 4.10.

Table 4.10: H_{fus} for the phase transitions occurring in TMATEA – $ZnBr_4$on heating and cooling.

T [°C]	H_{fus} [J/g]
217	33.84
215	27.65

4.6 TMATEA – $MnBr_4$

4.6.1 Observations of synthesis

The precursor solutions tetramethylammonium bromide and tetraethylammonium bromide were clear, however the manganese bromide tetrahydrate solution had a pinish color

which also was retained in the final mixed solution. The initial crystallization, Figure 4.22a, started after 24 hours and exhibited small square-like yellow crystals with a size of approximately 9 mm^2 and thickness of 1 mm. The solution retained the pinkish color and some particles of with the same color as manganese bromide tetrahydrate powder is to be seen in Figure 4.22a in the lower left part of the crystallization dish. The final dried product, Figure 4.22b, was agglomerates of crystals as the ones in Figure 4.22a. Some of the variation in size and shape distribution for the final product is shown in Figure 4.22c.

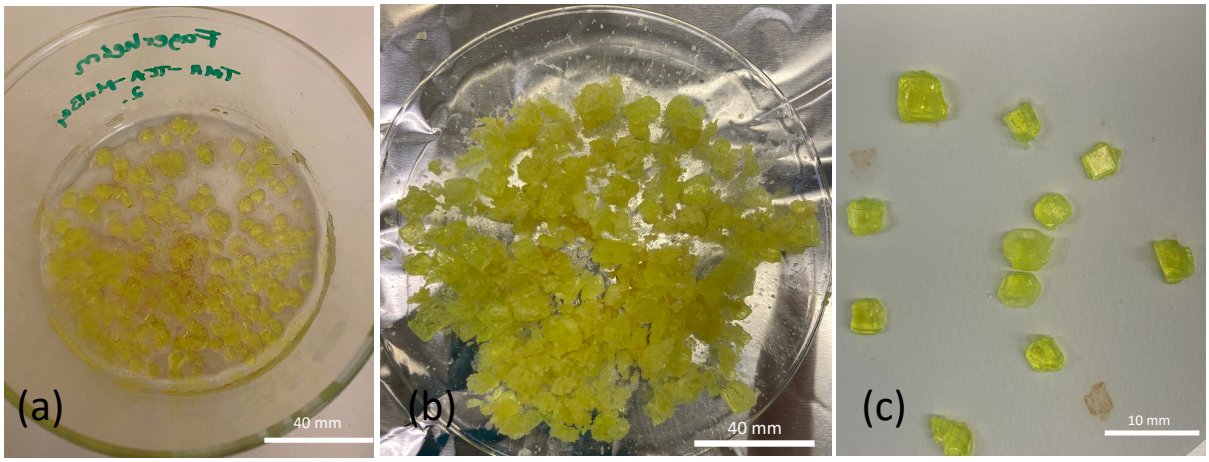

Figure 4.22: Crystal morphology of TMATEA – $MnBr_4$ crystals formed by slow evaporation. (a) Initial crystallization, (b) dried product and (c) single crystal.

4.6.2 Crystal structure

The diffractogram for TMATEA – $MnBr_4$ powder is given in Figure 4.23 including the fitted pattern and the difference between these two. The crystallographic information at room temperature for the compound is given in Table 4.11. These values were determined by Rietveld-refinement using TOPAS. The Goodness of fit (GOF) is included in the Table 4.11 and is an indication on how well the refinement fits to the diffractogram for observed data of the crushed TMATEA – $MnBr_4$ and has a value of 9.53. The structure is determined to have a tetragonal lattice with space group P21m and lattice parameters a=b=13.647 Å and c=12.154 Å which differ from the values reported by Szklarz *et al.*[28] with respectively +0.025 and +0.016.

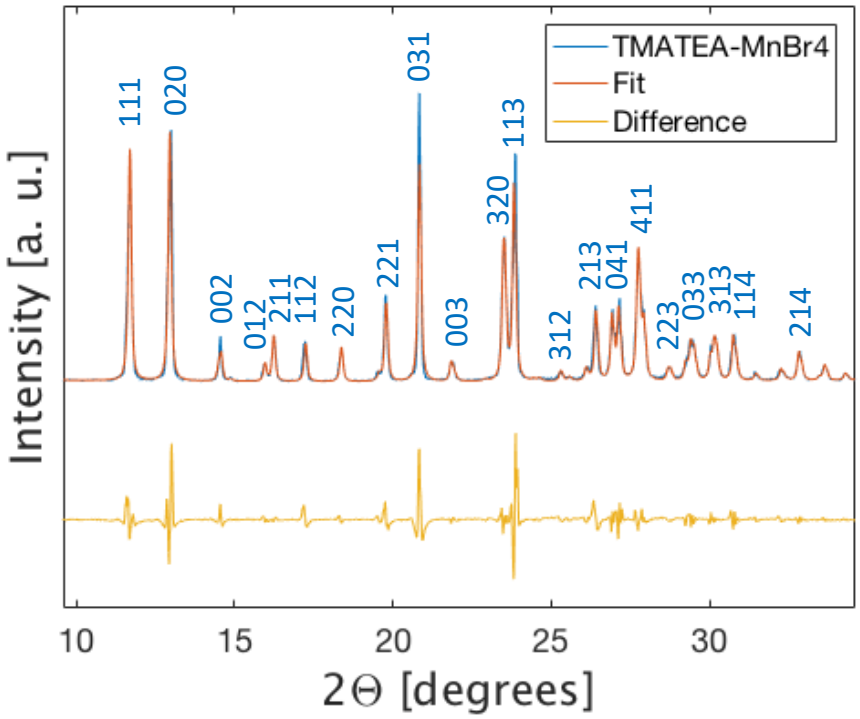

Figure 4.23: Diffractogram for TMATEA – $MnBr_4$ powder including the diffractogram for the fit done by Rietveld-refinement and difference between these two. The Miller indices are given on top of the corresponding peak.

Table 4.11: The crystallographic information at room temperature for TMATEA – $MnBr_4$.

TMATEA – $MnBr_4$	
Temperature [K]	295
Crystal system	Tetragonal
Space group	P21m
a [Å]	13.6473
b [Å]	13.6473
c [Å]	12.1543
V [$Å^3$]	2263.7261
GOF	9.53

A crytallographic information file (CIF) for TMATEA – $MnBr_4$ was used to illustrate the structure in VESTA as one can see in Figure 4.24.

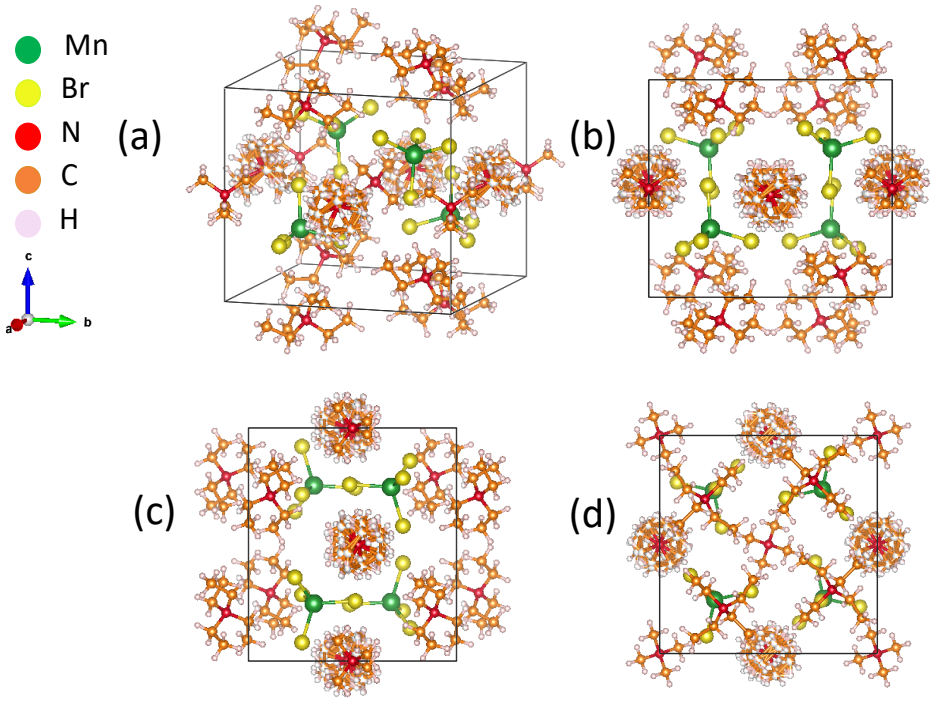

Figure 4.24: Crystal structure for TMATEA – $MnBr_4$ illustrated in different directions. (a) shows the standard unit cell aligned according to the axis arrows show. Each additional figure shows a perspective of the structure with a specific axis coming out of the page (b) the A-axis, (c) the B-axis and (d) the C-axis.

The structure is similar to the one described for TMATEA – $ZnBr_4$ in Section 5.5.2 except for the anion which in this stucture is $[MnBr_4]^{2-}$

4.6.3 Phase transitions

To determine the thermal behaviour of the compound DSC measurements was performed during heating and cooling from -25 °C to 240 °C for three cycles. Figure 4.25 shows an anomaly characteristic for reversible first-order phase transition occur at 215 °C and 210°C on heating and cooling respectively with a relatively small temperature hysteresis of 5 °C. Szklarz *et al.*[28] has reported transition at 211 °C and 209 on heating and cooling respectively. The peak around -20 °C is an artefact from the measurement and is therefore not studied further.

The enthalpy of transition, H_{fus}, indicate the amount of energy each transition releases or absorbs. Using Figure 4.25 H_{fus} is determined by calculating the area under the corresponding peak with the same method as described in Section 4.5.3 for TMATEA – $ZnBr_4$. These values are given in Table 4.12.

Table 4.12: H_{fus} for the phase transitions occurring in TMATEA – $MnBr_4$ on heating and cooling.

T [°C]	H_{fus} [J/g]
215	33.84
210	17.95

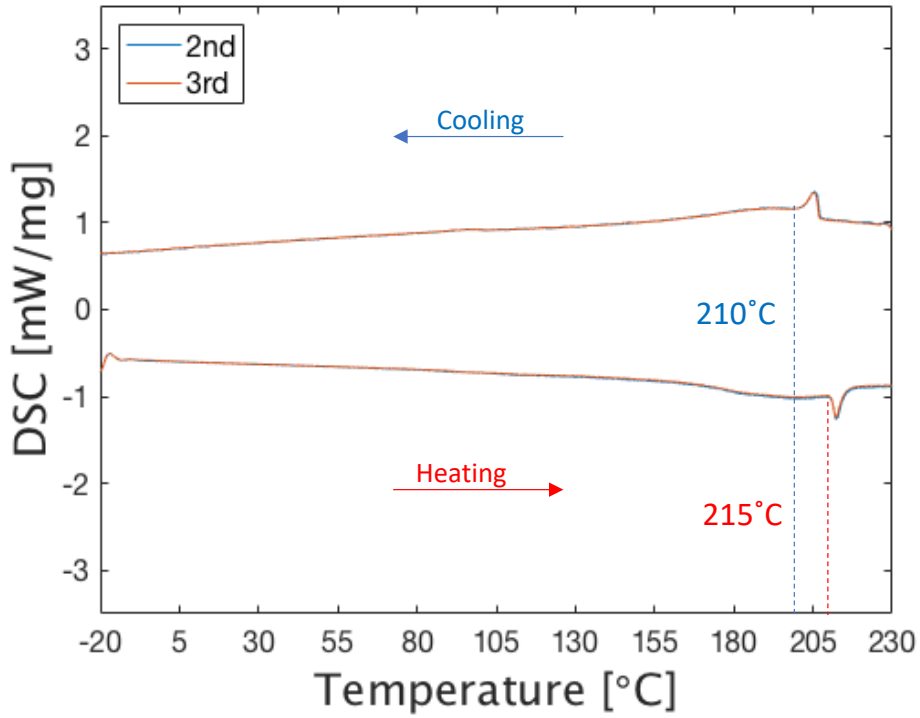

Figure 4.25: DSC results for TMATEA – $MnBr_4$ crystals. The sample was cycled between -25 °C and 240 °C three times (the fist cycle is not included). The phase transitions are marked with red and blue dotted lines for heating and cooling respectively.

5 Discussion

The main results presented are related to the crystal morphology, structural composition and phase transitions of the six compositions TMA – $ZnBr_4$, TMA – $MnBr_4$, TEA – $ZnBr_4$, TEA – $MnBr_4$, TMATEA – $ZnBr_4$ and TMATEA – $MnBr_4$. Thus, the discussion will be broken into three sections: Crystal morphology, crystal structure and phase transitions where the compositions will be compared to indicate the influence of the organic cations and the inorganic anions on the properties.

5.1 Crystal morphology

Observation of the growth of the six compounds reveals a very different crystal habit. The temperature, concentration of the solution and the conditions for evaporation, specifically the humidity and the size of the crystallization dish, were the same thus it can be neglected in the comparison of the crystal growth of the six compounds[16].

By looking on the compounds exhibiting the same cations the TMA-compounds differ as the TMA – $ZnBr_4$ crystals are clear, small with smooth faces and hexagonal geometry while the TMA – $MnBr_4$ crystals are yellow, with rough faces and dendritic geometry. This difference indicates variations in the growth rate of the different crystallographic faces where the dendritic growth indicates a highly anisotropic growth rate depending on the crystallographic direction. There are several factors influencing the crystal morphology. First and foremost there are different precursors, $ZnBr_2 \cdot 2\,H_{20}$ and $MnBr_2 \cdot 4\,H_{20}$, used in combination with TMABr. However, both degree of supersaturation and impurities of the supersaturated solution are also playing a role of the final crystal morphology[16].

For the TEA-compounds the crystal habit is quite different. The crystal growth of TEA – $ZnBr_4$ results in crystals with a big variation in size and shape as most of the crystals look like powder and some are big single crystals with an face area of 4 cm^2. The single crystals are quadratic and one can see the growth steps as diagonals from the center to the four edges (Figure 4.9 (c)) with horizontal lines parallel to the edges within the diagonals. The initial crystallization were only single crystals while as the excessive water evaporated the crystal growth changed to smaller powder-like crystals. Therefore the difference in crystal habit within the compound can originate from an decreased growth rate as the concentration of the solution changes when excessive water evaporates. On the other hand the crystal habit is very different from the TEA – $MnBr_4$. These crystals have various shapes from quadratic to hexagonal and the size is inconsistent. The TEA-molecule is fluctuating between two orientations. Either of these two orientations will reduce the symmetry of the lattice and will decrease the volume occupied by the TEA-molecule[23]. Can the variation in crystal habit can originate from the two different orientations the TEA-molecule can have which will make the nucleation and growth rate different? Or the fact that the additional degree of freedom compared to TMA leads to a lower amount of energy needed to nucleate? This is two questions which needs more investigation.

For the TMATEA-crystals the size and shape distribution is continuous throughout the whole crystallization which results in homogeneous crystal size and shape.

TMATEA$-ZnBr_4$ crystals, as for TMA$-ZnBr_4$, have a hexagonal shape. Also the TMATEA$-MnBr_4$ have a small size distribution and the shape is a mix of quadratic and hexagonal-like crystals (Figure 5.21 (c)) and is quite similar to the TEA$-MnBr_4$ crystals. The continuous growth suggests a stable molecule which leads to a continuous amount of energy needed to nucleate throughout the whole crystallization process.

To indicate how the cation influences the crystal morphology the crystals with the same anion are compared. For the [A_2-ZnBr_4]-compounds where A is TMA and/or TEA the crystal habit of TMA$-ZnBr_4$ and TMATEA$-ZnBr_4$ is quite similar while the habit for the TEA$-ZnBr_4$ crystals is very different both in shape and size. This suggests that the cations do have a role in the crystal habit and the TEA-cation with it's orientational freedom which may play a role in the nucleation and nucleation energies. On the other hand comparing the crystals exhibiting the same cations one can easily spot the difference in shape, size and color which suggests the anion is more influential on the crystal growth than the two organic cations used.

The similarities throughout all the compositions is the color for the compounds with the same anion as the $[ZnBr_4]^{2-}$- compounds are colorless and the $[MnBr_4]^{2-}$ are yellow after drying. After vacuum filtration a colour change was observed for the A_2-MnBr_4 crystals, where A is TMA and/or TEA. Before removing the excessive water the crystals exhibited a pinkish-orange colour while after removal they turned yellow. Optical properties of crystals are caused by the electronic structure, which can interact and absorb specific wavelengths of light and change the wavelength of light emitted. To be more specific it is the number of electrons of the transition metal in the anions that is giving the color. The ligand field from the surrounding halide can modify the wavelength and give the crystals different colors.

5.2 Crystal structure

The cell volumes for the six compositions are compared in Figure 5.1. As expected the volume increases from TMA-compounds, mixed TMA-TEA to the TEA-compounds due to a larger volume for the TEA-molecule. One exception is TEA$-ZnBr_4$ which has the significantly smallest volume. As one can see in Figure 5.1 the difference in volume between TEA$-ZnBr_4$ and TEA$-MnBr_4$ is the biggest one. This difference can originate from the ability this molecule has to rotate. As reported in literature[23] the TEA molecules are less spherical in terms of the space it occupies. The difference in symmetry within the TEA-compounds is well illustrated in Figure 4.11 and Figure 4.15 in Chapter 4 where TEA$-ZnBr_4$ has a rectangular structure while the TEA$-MnBr_4$ has a more quadratic one. The rotational freedom difference ultimately accounts for the large difference in the volumes in the two TEA materials and as the rotational freedom plays a strong role in the volume of the organic cation and the ultimate structure of the material this then likely explains the why the volume of TEA$-ZnBr_4$ is also lower than even the TMA compositions.

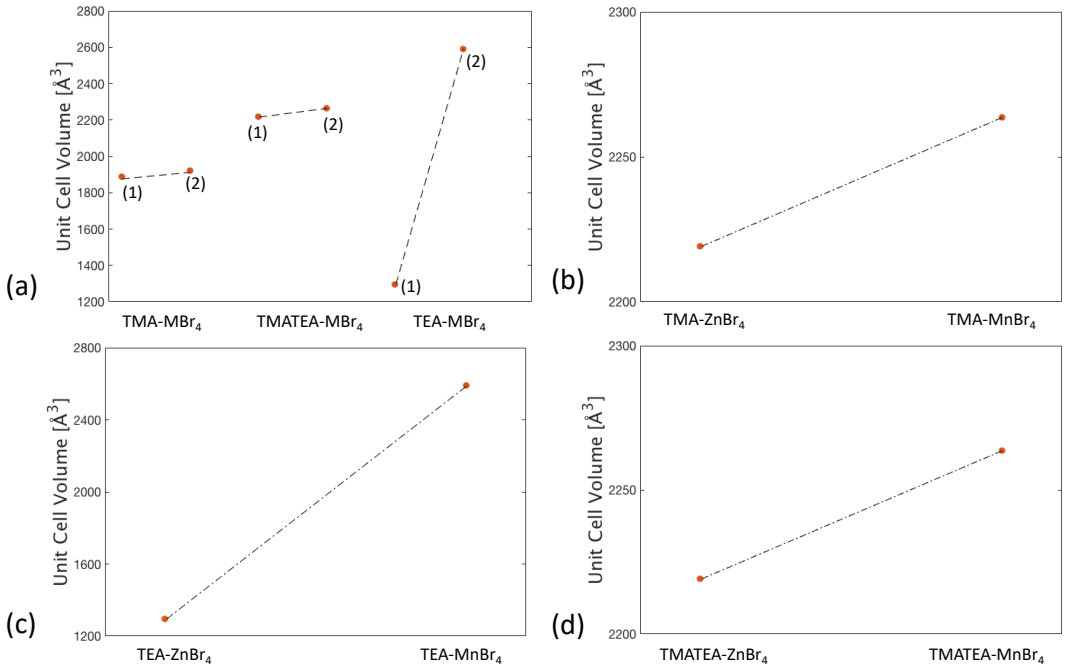

Figure 5.1: Comparison of the unit cell volume(ucv) for the compositions. (a) The dots are placed above the corresponding composition where (1) has M=Zn and (2) has M=Mn. (b)Ucv for TMA-compounds (c)TEA-compounds (d)TMATEA-compounds.

As indicated in Figure 5.1 the A_2MnBr_4-compositions do have a larger volume than the A_2ZnBr_4-compositions. By plotting the compositions with the same cation against each other, as in Figure 5.2, it is clear that the Mn-based compound have a bigger volume. This is consistent with the fact that the $[MnBr_4]^{2-}$ anion has a larger ionic radius than the $[ZnBr_4]^{2-}$ anion, corresponding with the ionic radii of the metal ions respectively 161 and 142 pm.

The structure of the compositions were determined by XRD and are presented in Chapter 4. To study how the cations or anions influence the crystal structure the compositions are plotted against each other by first fixing the cations (Figure 5.2) and then fixing the anions (Figure 6.3). In Figure 5.2, when fixing the organic cations, the structure is quite similar for both anions for the TMA and TMATEA-compounds. For the TEA-compounds the diffractogram differ for the two anions which is also indicated in Section 4.3 and 4.4 by the two compositions having different space groups. It is suggested that the difference in symmetry originate from the additional degree of freedom the TEA-cation exhibit compare to the TMA-cation. Some additional peaks are to be seen for $TMA-MnBr_4$, as also mentioned in Section 4.2.2, these are suggested to belong to one of the precursors (TMABr).

In Figure 5.2, when fixing the cation, the structure is quite similar for both anions for the TMA and TMATEA-compounds. For the TEA-compounds the diffractogram differ for the compositions as a function of the anion used which is also indicated in Section 4.3 and 4.4 by the two compositions having different space groups.

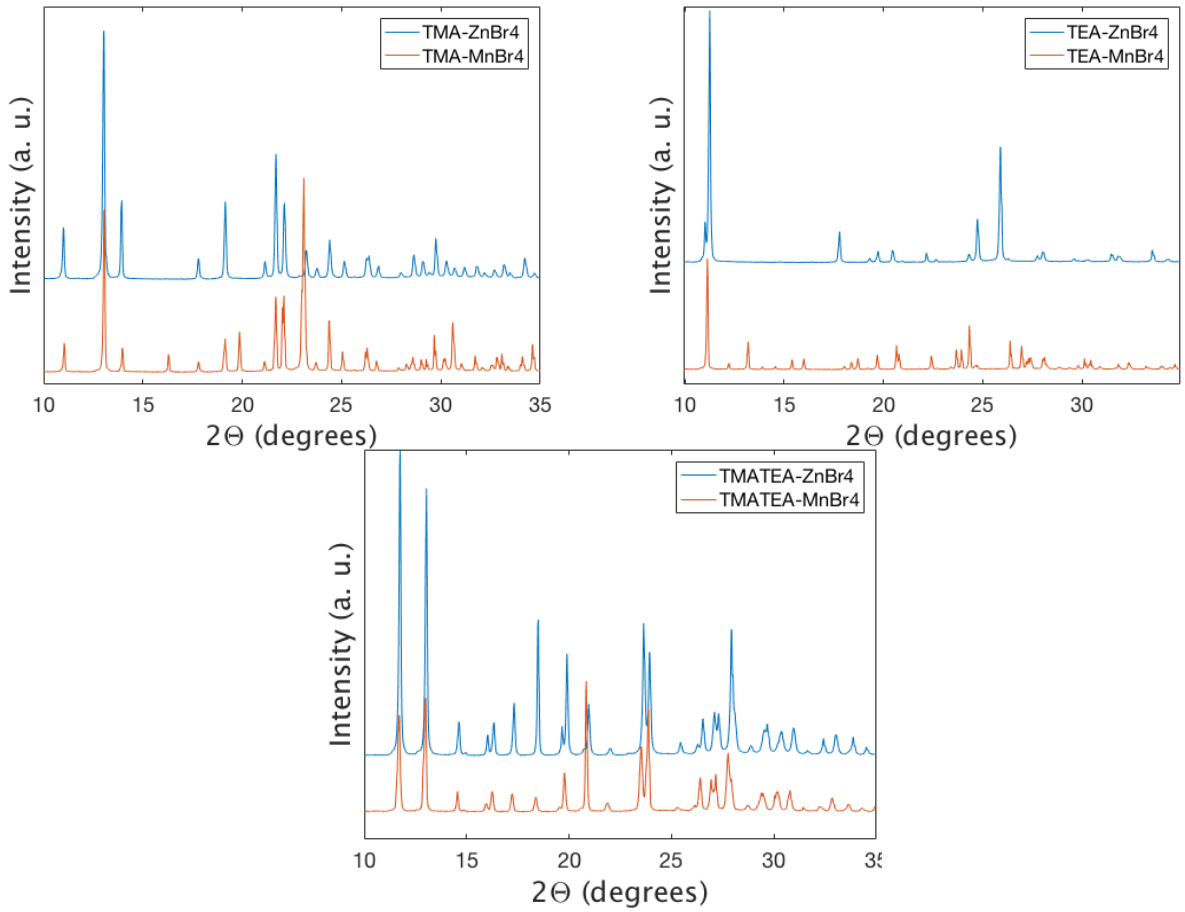

Figure 5.2: Diffractograms for the compositions with the same cations compared. (a) Compositions with TMA as cations (b) TEA (c) TMATEA.

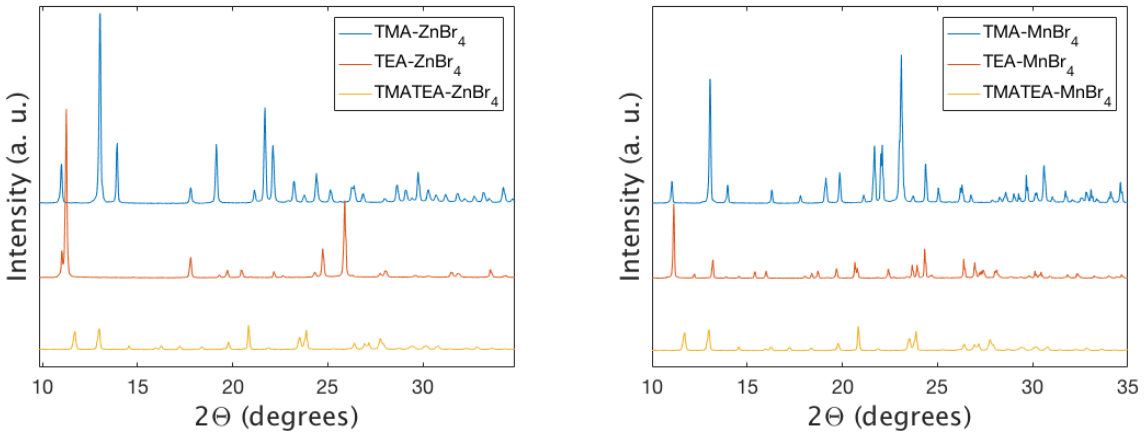

Figure 5.3: Diffractograms for the compositions with the same anion compared. (a) Compositions with $[ZnBr_4]^{2-}$ as anion. (b) Compositions with $[MnBr_4]^{2-}$ as anion.

In Figure 5.3 the anions are fixed and the cations are varied. These diffractograms varies

significantly more than the ones in Figure 5.2. This is an indication of that the cations play the major role in the structural design of the crystals which seems reasonable since they vary in size quite considerably.

5.3 Phase transitions

Differential scanning calorimetry (DSC) is a calometric technique for determination of phase transitions and are helpful to gain understanding about how these contribute to the characteristics and properties of the materials[31]. In chapter 4 the DSC data were presented for each of the six compositions investigated in this work. In this section these data are discussed in comparison to determine how the cation and anion compositions respectively influenced the temperature, number of and characteristics of the phase transitions taking place.

The characteristic of the peak is an indication on what type of transition the material undergoes. The peaks on heating for the A_2-ZnBr_4 where A is TMA and/or TEA is enlarged in Figure 5.4. For TMA$-ZnBr_4$ the peak is diffuse without a sharp peak (Figure 5.4a). This phase transition is reported in literature as a second-order phase transition[19]. The TEA$-ZnBr_4$ crystals undergo two transitions with sharp peaks as one can see in Figure 5.4b. The DSC peak for TMATEA$-ZnBr_4$ (Figure 5.4c) shows an anomaly phase transition as it includes both a diffuse peak and a sharp peak. This combination is indicating first a pre-transitional contribution which is related to a order-disorder transition followed by the sharp peak related to a displacive type of phase transition[27]. The variation in identity as illustrated in Figure 5.4, and the lack of variation when the compositions exhibiting the same cations, indicates that the cations play the major role in the identity of the phase transitions. In addition the TEA-compounds undergoes two phase transitions, in the studied temperature range, while TMA- and TMATEA-compounds undergoes one. The TEA-cation does have an additional degree of freedom compared to that of the TMA-cation which can explain the additional phase transition as also reported in literature[32].

When comparing the compositions with the same cations, TMA, TEA and TMATEA, the temperature for when the transitions occur does not show a trend. The literature suggests that the largest organic molecule should have the highest transition temperature, since the transition is driven by molecular rotation and more energy is needed to rotate the larger TEA molecule[23]. However Kahrizi *et al.* reports interesting results from a EPR study about the A_2MBr_4-crystals. In this study it was found that for the TMA-compounds the number of phase transitions occurring and the corresponding phase transition temperature decrease as the radius of the metal ion increase. As for the TEA -compounds these dependences were opposite to those observed for TMA compounds[24]. This is not consistent with the results in this project where the phase transition temperatures for the the A_2MnBr_4 is lowest both for the TMA- and TEA-compounds while the TMATEA-compounds shows the opposite. The conflict between the literature and the results in this thesis suggests a weak correlation between the two anions studied and the transition temperature, instead pointing to the cations as the main determining factor.

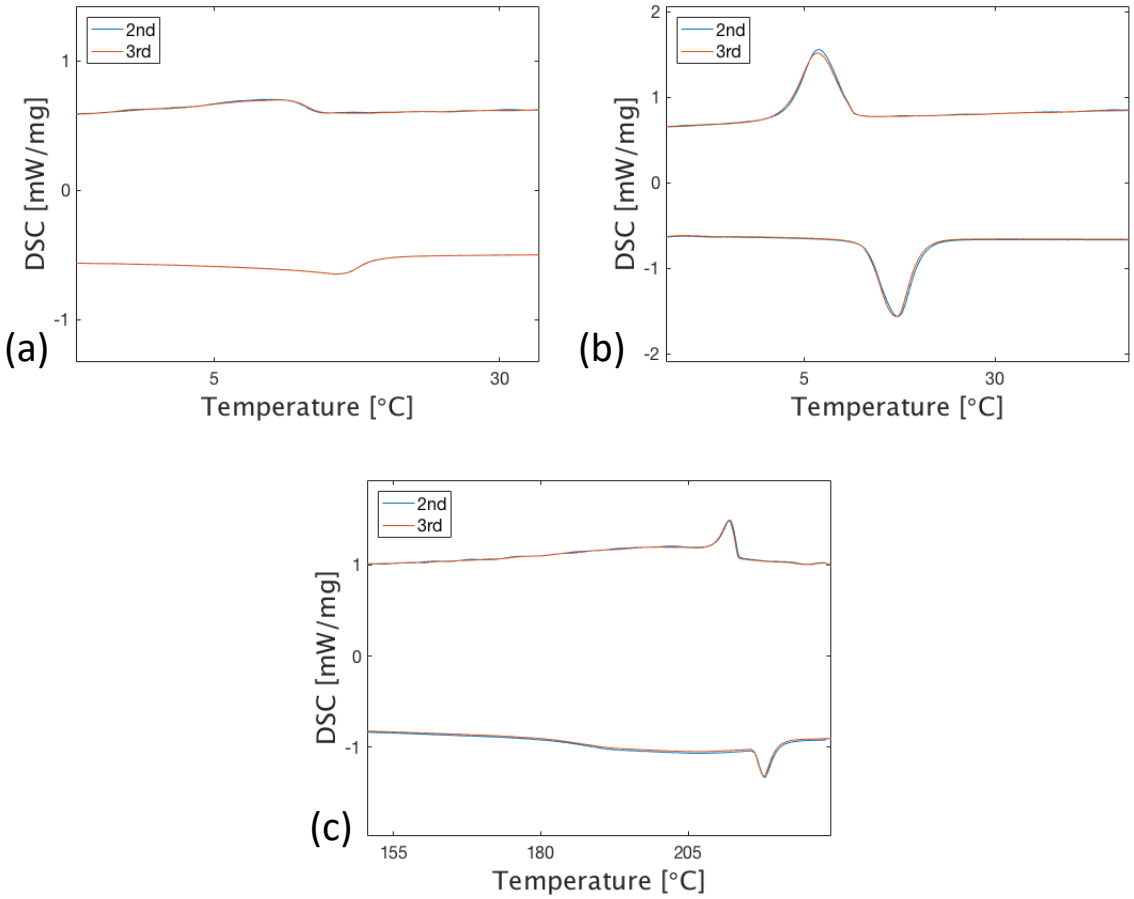

Figure 5.4: DSC peaks for the A−$ZnBr_4$ compounds where A is TMA and/or TEA. (a) TMA−$ZnBr_4$ (b) TEA−$ZnBr_4$ (c) TMATEA−$ZnBr_4$.

The DSC measurements indicates when energy is released or absorbed by the material as a function of temperature. These materials are going trough solid-solid phase transitions as a function of temperature than involve increasing the molecular orientational freedom and changing the symmetry of the structure. Thee thermal energy allows the lattice to expand creating space for the molecular rotation. By analyzing the DSC-curve the enthalpy of fusion,H_{fus}, can be determined. To determine H_{fus} the area under the specific peak is calculated[33,34]. A positive peak indicates an exothermic reaction and a negative peak an endothermic reaction in the sample.

The enthalpy of the transition, ΔH_{fus}, has small variations within the compositions exhibiting the same cations, as illustrated in Figure 5.5. The one exception is for the second phase transition for TEA−$MnBr_4$ which has a significantly larger ΔH_{fus} than TEA−$ZnBr_4$. This large difference is not present in the other compositions, exhibiting the same cations, thus it is not likely due to the changed anion. Possibly it is due to the rotational freedom the TEA-cation exhibit which leads to this large difference in the energy needed to break the structure and undergo the transition. However, in order to confirm this and understand why this large change is observed in TEA−$MnBr_4$ and not TEA−$ZnBr_4$ it is necessary to examine the high temperature structure, which is proposed

as future work.

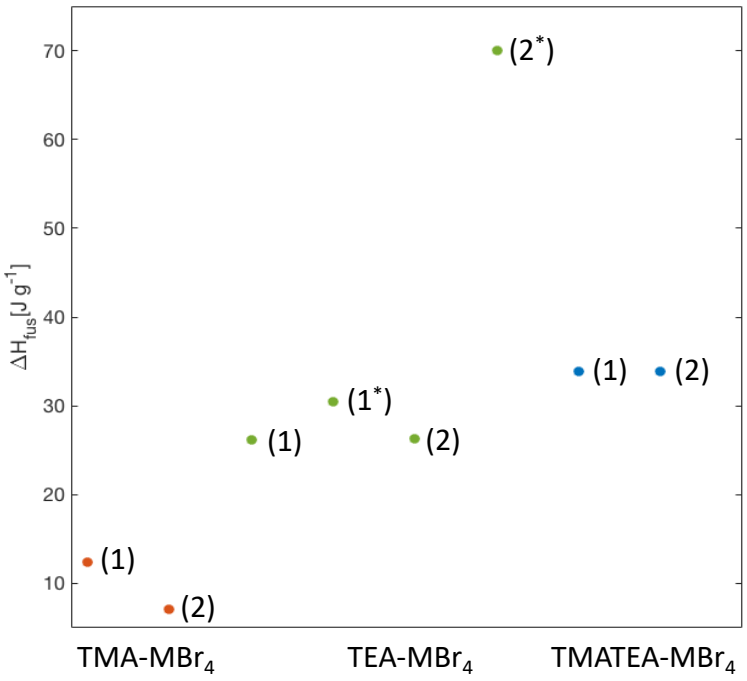

Figure 5.5: The enthalpy of fusion, ΔH_{fus}, on heating for the six compositions. The cations for the compositions is indicated by colors where TMA-comppounds are orange, TEA are green and TMATEA are blue while the anion (M) is indicated by numbers where (1): M=Zn and (2): M=Mn. The TEA-compounds exhibit two phase transitions where the second one is marked with a *.

As reported in Chapter 4 there is some hysteresis in the ΔH_{fus} for the exothermic and endothermic transitions. This suggests that the diffuse nature of the phase transitions means that it is possible some part of the transitions are not visible in the measurements and thus leads to error in the calculation.

6 Conclusion

In this thesis the main goal was to determine the influence of the compositional design on the crystal morphology, structural- and thermal properties. This was done by mixing two cations, TMA and TEA, and two anions, $[ZnBr_4]^{2-}$ and $[MnBr_4]^{2-}$, into six different compositions the influence of the cations and anions. The analysis on how the cation and anion influenced the properties was done by observation of the crystal growth, XRD and DSC analysis of all of the compositions.

- The cation size had a large effect on the structure of the materials, effectively changing the symmetry and space group of the material.
- The anion used had a noticeable but smaller effect, producing a volume change in the unit cell corresponding to the anion size.
- A complex array of phase transitions was observed between -25 and 280 °C displaying both order-disorder and displacive characteristics depending on the composition. The organic cation played the largest role in influencing this behaviour.

7 Further work

The research on the influence of the cations and anions on crystallization, structure and thermodynamics are limited, thus further investigation is required to determine the full potential for the A_2MBr_4-crystals.

- Optical polarizing microscopy to determine possible domains in the structure. To check whether the crystals studied have a high-temperature ferroelastic domain structure would provide valuable information about the nature of the observed phase transitions.
- Determine the electrical properties of the crystals through dielectric measurements.
- XRD measurements at other temperatures to determine gain information about the structure in other phases.
- Develop a method to investigate the characteristics of the phase transitions.
- DSC measurements at a larger temperature range to determine if there are more phase transitions occurring.

References

[1] K. Fagerheim. Organic-inorganic supramolecular plastic crystals. *TTMT4500 Specialication project (NTNU)*, 42:1–42, 07 2020.

[2] P. Atkins and T. Overton. *Shriver and Atkins' Inorganic Chemistry*. OUP Oxford, 2010.

[3] J. Pringle, P. Howlett, D. MacFarlane, and M. Forsyth. Organic ionic plastic crystals: Recent advances. *J. Mater. Chem.*, 20, 03 2010.

[4] J. Timmermans. Plastic crystals: A historical review. *Journal of Physics and Chemistry of Solids*, 18(1):1–8, 1961.

[5] M. Zelzer and R.V. Ulijn. 6 - enzyme-responsive polymers: properties, synthesis and applications. pages 166 – 203, 2014.

[6] A. Tayi, A. Kaeser, M. Matsumoto, T. Aida, and S. Stupp. Supramolecular ferroelectrics. *Nature chemistry*, 7:281–294, 03 2015.

[7] K. Takashi. Supramolecular liquid-crystalline materials: molecular self-assembly and self-organization through intermolecular hydrogen bonding. *Supramolecular Science*, 3(1):53 – 59, 1996.

[8] X. Dong, C. Hsu, Y. Li, H. Liu, J. Wang, M. Huang, K. Yue, H. Sun, C. Wang, X. Yu, W. Zhang, B. Lotz, and S.Z.D. Cheng. *Supramolecular Crystals and Crystallization with Nanosized Motifs of Giant Molecules*. Springer International Publishing, 2017. ISBN 978-3-319-49203-2.

[9] J. Walker, R. Miranti, S. Skjærvø, T. Rojac, T. Grande, and M. Einarsrud. Supercoercive electric field hysteresis in ferroelectric plastic crystal tetramethylammonium bromotrichloroferrate(iii). *Journal of Materials Chemistry C*, 01 2020.

[10] N. Løndal. Effects of material structure on the electrical properties of ferroelectric plastic crystal tetramethylammonium bromotrichloroferrate(iii). *Master thesis, NTNU*, 2020.

[11] H. Ye, J. Ge, Y. Tang, P. Li, Yi Zhang, Y. You, and R. Xiong. Molecular ferroelectric with most equivalent polarization directions induced by the plastic phase transition. *Journal of the American Chemical Society*, 138(40):13175–13178, 2016.

[12] R.A. Lim. Study of the ferroelastic phase transition in the tetraethylammonium compound [n(c2h5)4]2znbr4 by magic-angle spinning and static nmr. *AIP Advances*, 6(3):035307, 2016.

[13] R.J.D. Tilley. *Understanding Solids: The Science of Materials, 2nd Edition*. Wiley, 2013. ISBN 9781118423288.

[14] M. Helbæk and S. Kjelstrup. *Fysikalsk kjemi, 2nd edition*. Fagbokforlaget, 2006. ISBN 9788245004045.

[15] W.D. Callister and D.G. Rethwisch. *Materials Science and Engineering: An Introduction, 8th Edition*. Wiley. ISBN 9780470941669.

[16] J.W. Mullin. *Crystallization, 4th Edition*. Reed Educational and Professional Publishing Ltd, 2001. ISBN 0750648333.

[17] A. López-Echarri, I. Ruiz-Larrea, and A. Fraile-Rodriguez. The thermoelastic properties of [n(ch3)4]2znbr4 and [n(ch3)4]2mnbr4. *Phase Transitions*, 71(2):101–111, 2000.

[18] K. Tanaka, T. Shimada, Y. Nishihata, and A. Sawada. Roles of cation and anion molecules in ferridistortive phasetransition in [a(ch3)4]2xbr4 type crystals. *Journal of the Physical Society of Japan*, 64(1):146–154, 1995.

[19] A. Takanao, H. Katsuhiko, and G. Kazuo. Refinement of the crystal structure of [n(ch3)4]2znbr4 in connection with its phase transition. *Journal of the Physical Society of Japan*, 57(12):4219–4224, 1988.

[20] A. Kiraci. Analysis of the specific heat and the free energy of [n(ch3)4]2znbr4 close to the ferro-paraelastic phase transition. *Phase Transitions*, 92(3):249–258, 2019.

[21] M. Iwata, M. Matsuda, and H. Orihara. Observation of the ferroelastic domain structure near the phase transition point. *Ferroelectrics Letters Section*, 21(5-6): 151–160, 1996.

[22] A. Takanao and H. Katsuhiko. Structure of tetramethylammonium tetrabromomanganate at room temperature. *Journal of the Physical Society of Japan*, 57(12): 841–843, 1988.

[23] A.J Wolthuis, W.J Huiskamp, and L.J De Jongh. Investigation of structural phase transitions in some $[N(C_2H_5)_4][MX_4]$ compounds, journal = Elsevier Science Publishers B.V., volume = 19, number = , pages = 301-319, year = 1986,.

[24] Misra S. Kahrizi, M. and J. Kotlinski. Mn2+ epr study of phase transitions occurring in single crystals of [n(ch3)4]2zncl4, [n(ch3)4]2znbr4, [n(ch3)4]2cobr4, [n(c2h5)4]2zncl4, [n(c2 h5)4]2znbr4, [n(c2h5)4]2cobr4 and [n(c2h5)4]2mnbr4. *Solid State Communications*, 79.2:167–173, 1991.

[25] P. Sondergeld, H. Fuess, A. Mason, H. Ishiharab, and W. Schmahlc. Pseudosymmetries of the phases of (et4n)2znbr4. *Institute of Materials Science, University of Technology, Darmstadt, Germany*, page 9, 2000.

[26] S. Chen, J. Gao, J. Chang, Y. Zhang, and L. Feng. Organic-inorganic manganese (ii) halide hybrids based paper sensor for the fluorometric determination of pesticide ferbam. *Sensors and Actuators B: Chemical*, 297:126701, 2019.

[27] M.K. Krawczyk, A. Ingram, R. Cach, Z. Czapla, O. Czupiński, S. Dacko, and P. Staniorowski. Unusual structural phase transition in [n(c2h5)4][n(ch3)4][znbr4]. *Phase Transitions*, 91(4):356–369, 2018.

[28] Przemyslaw Szklarz, Adam Ingram, Z. Czapla, C. Górecki, and Marek Szafrański. Ferroelastic phase transition in [(c 2 h 5) 4 n][(ch 3) 4 n]mnbr 4. *Phase Transitions*, 90:1–8, 11 2016.

[29] G. Kazuo. Phase transition in N (CH3)42mnbr4. *Journal of the Physical Society of Japan*, 52(8):2931–2935, 1983.

[30] S. Chen, J. Gao, J. Chang, Y. Zhang, and L. Feng. Ccdc 1897520: Experimental crystal structure determination. 2019.

[31] K. Lukas and P. K. LeMaire. Differential scanning calorimetry: Fundamental overview. *Resonance*, 14(8):807–817, 2009.

[32] J. Harada, T. Shimojo, H. Oyamaguchi, H. Hasegawa, K. Takahashi, Y.and Satomi, Y. Suzuki, J. Kawamata, and T. Inabe. Directionally tunable and mechanically deformable ferroelectric crystals from rotating polar globular ionic molecules. *Nature Chemistry*, 8, 07 2016.

[33] M. E. Brown. Determination of purity by differential scanning calorimetry (dsc). *Journal of Chemical Education*, 56(5):310, 1979.

[34] E. Moukhina. Enthalpy calibration for wide dsc peaks. *Thermochimica Acta*, 522 (1):96 – 99, 2011.

NTNU

Norwegian University of
Science and Technology